Turkish Journal of Earth Sciences

Manuscript 1927

Tectonic geomorphology of the south-eastern section of the Burdur-Fethiye Shear Zone, Western Taurides: morphotectonic framework of the Eşen Basin

İREM ELİTEZ

CENK YALTIRAK

TÜBİTAK

Turkish Journal of Earth Sciences

http://journals.tubitak.gov.tr/earth/

Research Article

Turkish J Earth Sci
(2024) 33: 503-529
© TÜBİTAK
doi:10.55730/1300-0985.1927

Tectonic geomorphology of the south-eastern section of the Burdur-Fethiye Shear Zone, Western Taurides: morphotectonic framework of the Eşen Basin

İrem ELİTEZ[1,*], **Cenk YALTIRAK**[2]

[1]Department of Geophysical Engineering, Faculty of Mines, İstanbul Technical University, İstanbul, Turkiye
[2]Department of Geological Engineering, Faculty of Mines, İstanbul Technical University, İstanbul, Turkiye

Received: 30.08.2023 • **Accepted/Published Online:** 03.03.2024 • **Final Version:** 12.07.2024

Abstract: The Eşen Basin is a transtensional basin located in the south-eastern section of the Burdur-Fethiye Shear Zone and includes a part of the Western Taurides to the east. This tectonically complex area is bounded by the back-arc region of the Hellenic Arc, the offshore Anaximander Mountains, the offshore Rhodes and Finike basins, the extensional Western Anatolian region, and the compressional regions of the Western Taurides. In this study, in order to characterise the recent tectonic activity of the Eşen Basin, 101 drainage basins and 41 mountain fronts were analysed in terms of the longitudinal river profiles and the application of geomorphic indices: drainage basin asymmetry factor (AF), transverse topography symmetry factor (T), basin shape index (Bs), hypsometric curves and hypsometric integral (HI), valley-floor width to valley height ratio (Vf), mountain front sinuosity index (Smf), stream length gradient index (SL), and channel steepness index (k_{sn}). To improve the accuracy of the results of the indices, an index map of the relative tectonic activity (Iat) was created using the analytic hierarchy process (AHP), a multicriteria decision-making technique. In addition, the knickpoints, which indicate abrupt changes in the slope of river profiles, were identified to provide tectonic processes affecting the landscape. The comprehensive approach of this study unravels landscape dynamics of the Eşen Basin and the analyses suggest a high level of tectonic activity, especially in the northern and eastern sides of the basin, which is related to the surrounding tectonic features.

Key words: Burdur-Fethiye Shear Zone, Eşen Basin, Western Taurides, geomorphic indices, analytic hierarchy process, geomorphological analysis

1. Introduction

Geomorphology is a valuable source of information for understanding erosion processes and the activity of major faults within drainage systems. Geomorphic indices provide quantitative data to interpret landscape processes. The interplay between geomorphic indices and active tectonics is interconnected. Active tectonics plays a crucial role in controlling both uplift rates and river incision (Cox, 1994; Cowie et al., 2006). The evaluation of geomorphic indices in tectonically active basins helps to determine the anomalous basin behaviour. Therefore, the analysis of geomorphic indices has become a widely used method in regions recognized as tectonically active in recent years. These indices are commonly utilized to assess the relative tectonic activity of drainage basins in various studies (e.g., Bull and McFadden, 1977; Rockwell et al., 1985; Silva et al., 2003; El Hamdouni et al., 2008; Alipoor et al., 2011). As technology progresses, the interpretation of geomorphic indices, which depict the morphological evolution of a region, has evolved using different methods. While in most studies the relative tectonic activity of a region is commonly interpreted using the arithmetic mean of the geomorphic indices (Iat method in El Hamdouni et al., 2008), this study adopts the analytic hierarchy process (AHP). This approach assigns necessary weighting factors by means of a preference matrix in which all identified relevant criteria are systematically compared (Saaty, 1977; Alipoor et al., 2011).

The study area and its environs are situated in south-western Türkiye, one of the most tectonically active areas of the eastern Mediterranean (Figure 1a). This region is characterized by various tectonic features, including the Aegean back-arc extension regime (McKenzie, 1978; Le Pichon and Angelier, 1979; Meulenkamp et al., 1988; Yılmaz et al., 2000), the westward tectonic escape of Anatolia (McKenzie, 1972), the compressional Western Taurides uplift (Aksu et al., 2009, 2014; Hall et al., 2009, 2014), the Subduction Transform Edge Propagator (STEP) fault zone (Govers and Wortel, 2005; Hall et al., 2014), and the left-lateral transtensional Burdur-Fethiye Shear Zone (Elitez and Yaltırak, 2014a, 2014b, 2016; Elitez et al., 2016; Elitez and Yaltırak, 2023). Mostly NE-SW-striking active faults

* Correspondence: elitezi@itu.edu.tr

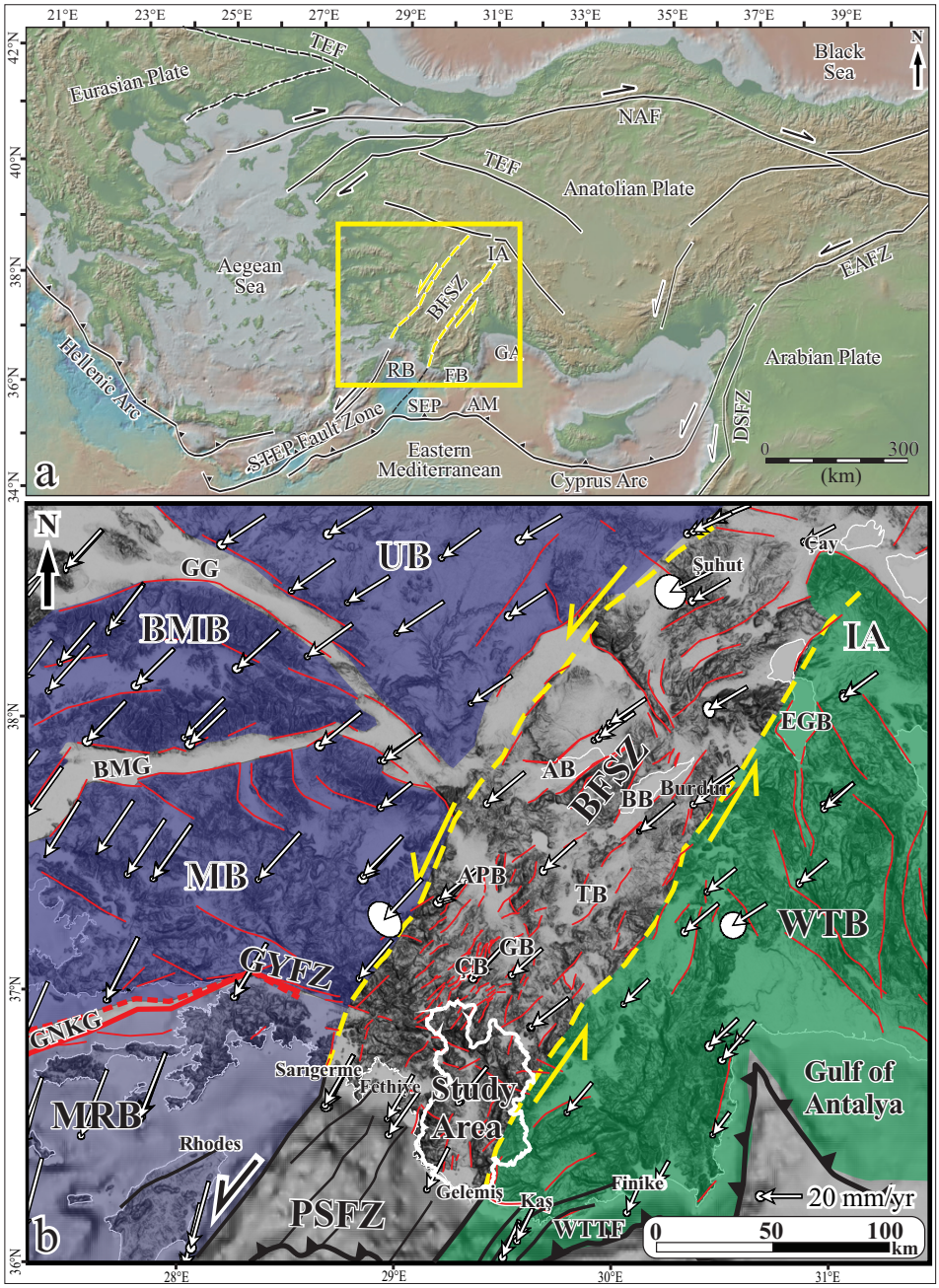

Figure 1. (a) Simplified tectonic map of Türkiye (BFSZ: Burdur-Fethiye Shear Zone, IA: Isparta Angle, TEF: Thrace-Eskişehir Fault, NAF: North Anatolian Transform Fault, EAFZ: East Anatolian Fault Zone, DSFZ: Dead Sea Fault Zone, RB: Rhodes Basin, GA: Gulf of Antalya, FB: Finike Basin, AM: Anaximander Mountain, SEP: Sırrı Erinç Plateau). Yellow rectangle indicates boundary of Figure 1b. (b) Regional fault map of south-western Anatolia compiled from Tur et al. (2015). Dark-blue region shows the NE-SW extensional domain (MRB: Marmaris-Rhodes Block, MB: Menderes Block, BMB: Büyük Menderes Block, UB: Uşak Block, GG: Gediz Graben, BMG: Büyük Menderes Graben, GNKG: Gökova-Nisyros-Karpathos Graben). Green region denotes the NNE-SSW compressional domain (WTB: Western Taurides Block, IA: Isparta Angle, WTTF: Western Taurides Thrust Fault). GPS vectors are from Kreemer et al. (2014). PSFZ: Pliny-Strabo Fault Zone, GYFZ: Gökova-Yeşilüzümlü Fault Zone, AB: Acıgöl Basin, BB: Burdur Basin, TB: Tefenni Basin, EGB: Eğirdir Basin. Yellow dashed lines indicate approximate boundary of the Burdur-Fethiye Shear Zone (BFSZ). White line indicates the boundary of the Eşen Basin.

have developed as a result of the N-S back-arc extension regime due to the roll-back of the Hellenic Trench and the counter-clockwise rotation of the western segment of the Aegean-Anatolian microplate. The Hellenic and Cyprus arcs, signifying the convergent boundary between the African Plate and Aegean-Anatolian Microplates, are connected by a tear in the subducting slab called the STEP fault zone (Govers and Wortel, 2005). The Burdur-Fethiye Shear Zone is the continuation of this STEP fault zone to the northeast through the Rhodes Basin and into south-western Anatolia (Taymaz and Price, 1992; Barka and Reilinger, 1997; Woodside et al., 2000; Huguen et al., 2001; Zitter et al., 2003; ten Veen, 2004; Aksu et al., 2009; Hall et al., 2009, 2014; Yaltırak et al., 2010; Ocakoğlu, 2012; Elitez and Yaltırak, 2023). The Burdur-Fethiye Shear Zone exhibits both northeast-southwest and northwest-southeast-striking normal and left-lateral oblique normal faults, with several basins being delineated by these major faults along the zone. The Eşen Basin is located in the south-eastern section of the Burdur-Fethiye Shear Zone, in a landslide prone region of the Western Taurides (Figure 1b).

This study addresses the lack of neotectonic observations in a commonly neglected region, the N-S-trending Eşen Basin. The focal point is to enhance our understanding of multiphase tectonic dynamics, including shear, compression, extension, and the evolution of drainage basins. The study examines various scales; the regional landscape, subbasins, drainage network, and sedimentary strata, aiming to conduct a thorough examination of the area. Geomorphological analyses were conducted to investigate the recent tectonic deformation processes and to determine the influence of the tectonic settings on the basin. The methodology involves a comprehensive analysis using geomorphic indices and the analytic hierarchy process (AHP) method. Field data, digital elevation model (DEM), geomorphic indices, and longitudinal river profiles are used in the assessment.

2. Geomorphological and geological features

The Eşen Basin is a N-S-trending Neogene basin with a length of approximately 65 km and a width of 35 km. The asymmetric topographic relief of the basin consists of lowlands to highlands ranging from a height of 0 to 2930 m (Figures 2 and 3a). Two different morphologies can be clearly defined in the Eşen Basin: 1) high mountains with steeper rivers in the eastern side, and 2) smaller hills with short rivers on the western side. The topography of the western side of the basin has a lower relief characterised by smaller hills and W-E- and NW-SE-trending wide valleys. To the east of the basin, the topography includes hills with very steep slopes. Broad alluvial plains lie in front of these hills. While the elevation decreases dramatically from north to south on the western side of the basin, the elevation difference is smaller on the eastern side (sections E-E' and F-F' in Figure 3a).

The drainage network of the Eşen Basin displays a complex dendritic pattern and a main channel, the Eşen River, running through the whole basin from north to south (Figure 2). It is dominantly characterized by short eastward flowing rivers (max. approximately 18 m) and longer westward flowing rivers (max. approximately 39 m). The longitudinal river profiles of the tributaries of the Eşen River reveal steeper channels in the eastern side of the basin (Figure 3b) cut by major faults. These rivers flow over basement rocks on the footwalls of the faults and continue over softer rocks on the hanging walls. However, in the western side of the basin, the rivers flow generally over alluvial deposits of wide valleys (Figure 2).

The area of gentle topography, dominated by a wide drainage system of the Eşen River, lies at the base of mountains and is underlain mainly by Neogene sediments (Figure 2). The highlands are prevailingly composed of the Mesozoic limestones of the basement. The lowlands are infilled by Upper Miocene-Lower Pliocene lacustrine deposits, indicating the presence of an ancient lake, and younger alluvial fan, talus, and alluvial deposits. The deltaic plain, on which the Gelemiş village is located, is characterised by Quaternary deposits carried by the Eşen River (Figure 2). Quaternary talus deposits covering the areas along the mountain fronts indicate recent fault activity.

The ages of the geological units in the study area indicate a broad time period between Palaeozoic and Quaternary. The basin is underlain by sedimentary units that unconformably overlie the basement rocks (Figure 4). These basement rocks are observed in the mountainous parts of the basin and consist of Palaeozoic to Paleogene Lycian Nappes (Brunn et al., 1970; Graciansky, 1972; Önalan, 1979; Ersoy, 1990), Lower Miocene-Eocene Yeşilbarak Nappe (Önalan, 1979) and Cretaceous to Lower Miocene Beydağları Para-autochthon (Şenel et al., 1989; Şenel, 1994, 1997), including ophiolitic mélange, limestone, flysch, sedimentary, and volcanic rocks. The younger sedimentary units comprise Upper Miocene to recent lacustrine marls, limestones, claystones, conglomerates, sandstones, alluvial fan deposits, talus deposits, and alluvial deposits (Figure 2; Elitez and Yaltırak, 2023).

The Eşen Basin is characterised by normal and oblique faults with left-lateral strike-slip components. These major faults indicate momentous geomorphic expressions both on the digital elevation model and in the field (Figure 5). The faults are identified as normal, oblique, normal fault without slickenside, and geomorphologically determined faults due to various indicators. The major faults in the Eşen Basin were mapped according to the field studies and

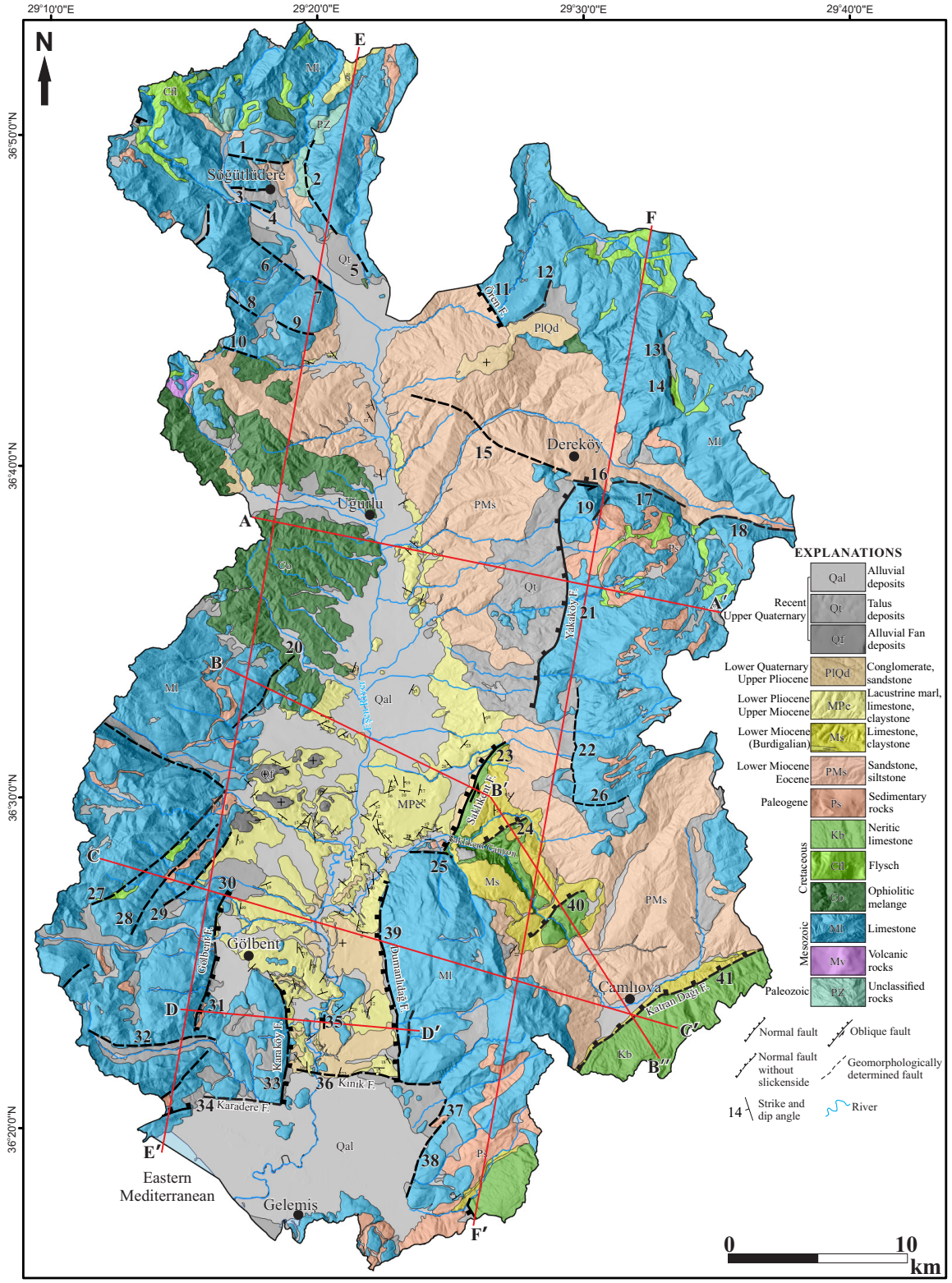

Figure 2. Geological map of the Eşen River Basin. Formation contacts were drawn by integrating field observations, DEMs, and satellite images. Ages of the basement rocks were derived from 1:500,000 Denizli sheet geological map of General Directorate of Mineral Research and Exploration (Şenel, 2002). Red lines indicate directions of geological and topographic sections in Figures 3 and 4. Numbers indicate the major faults in Figure 3a.

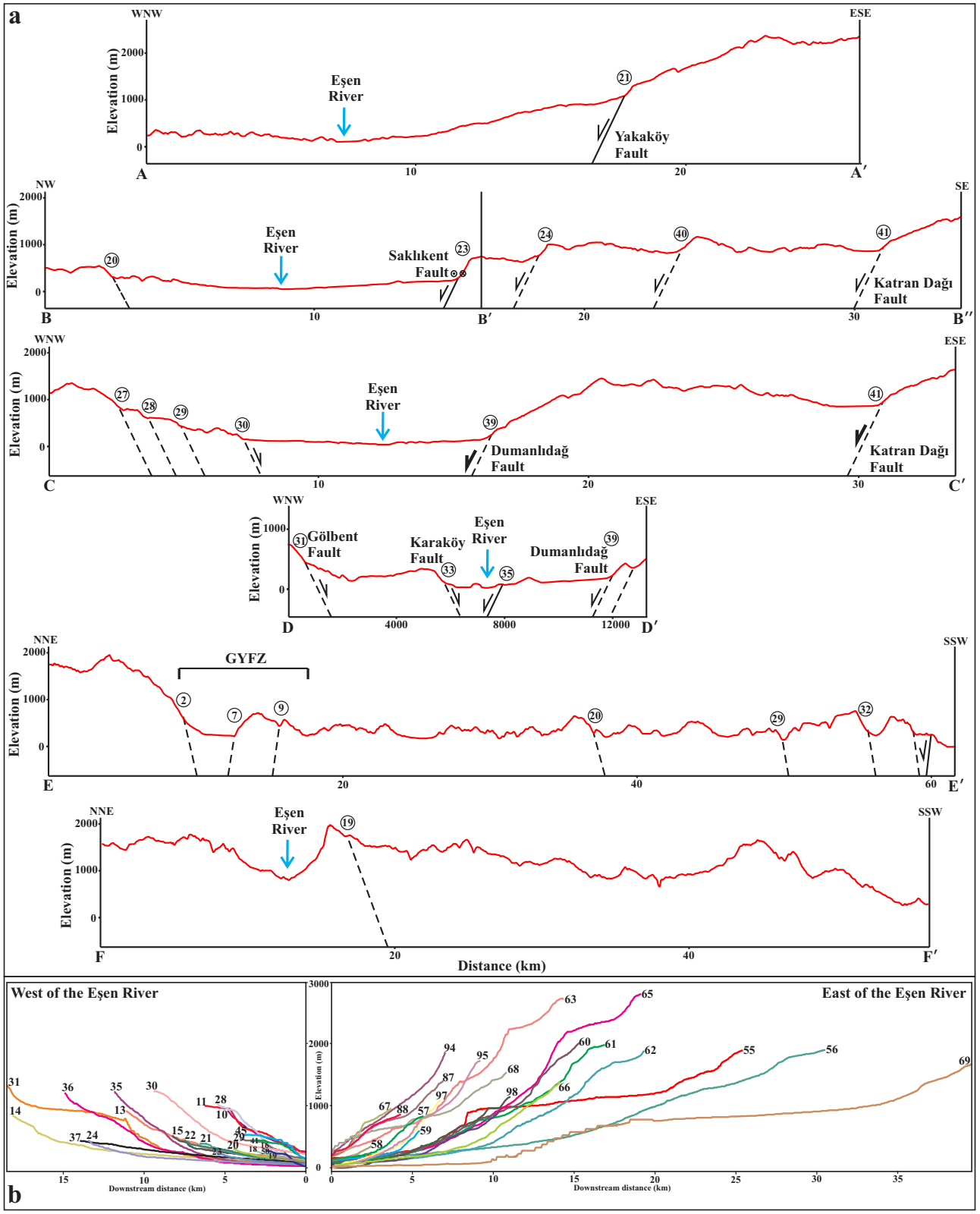

Figure 3. (a) Topographic profiles along the Eşen Basin. Locations of the profiles are shown in Figure 2. GYFZ: Gökova-Yeşilüzümlü Fault Zone. Numbers indicate the faults in Figure 2. (b) Exaggerated longitudinal river profiles on both western and eastern sides of the Eşen Basin. Numbers indicate the drainage basins in Figure 6.

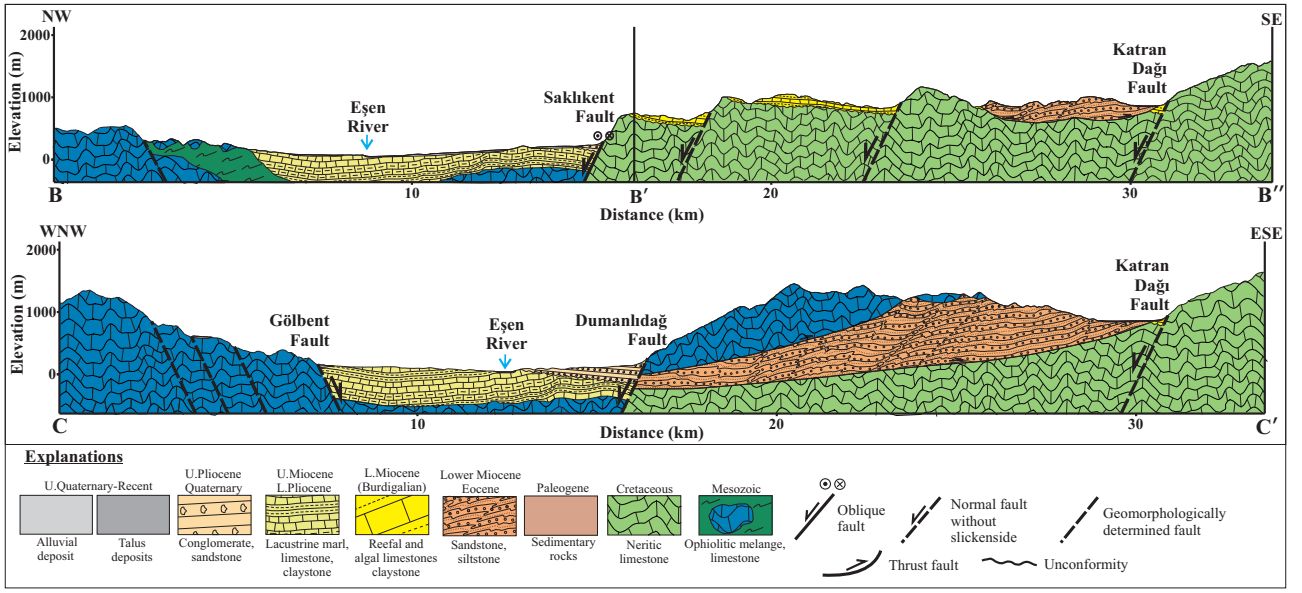

Figure 4. Geological cross sections through the study area (see directions in Figure 2).

the significant geomorphological expressions on DEM and airborne imagery. The faults are mainly NE-SW- and N-S-striking faults parallel to the main trend of the Burdur-Fethiye Shear Zone, or NW-SE- and W-E-striking faults parallel to the main trend of the Gökova-Yeşilüzümlü Fault Zone (Figure 2). Most of the NW-SE- and W-E-striking faults on the northern side of the Eşen Basin are the main faults of the Gökova-Yeşilüzümlü Fault Zone. This fault zone has been developed within the left-lateral shear zone between the southward thrusting of the Western Taurides, causing the subsidence of the offshore Rhodes and Finike basins (Hall et al., 2009) and the counter-clockwise rotation of the Menderes Block due to the back-arc extension of the Hellenic Arc (Tur et al., 2015; Elitez et al., 2016). The major faults of the Gökova-Yeşilüzümlü Fault Zone are the products of the shallow stresses largely reflecting the thrust and subsequent uplift of the Western Taurides (Figure 23 in Hall et al., 2009).

In the study area, although no striations were observed on some of the major faults, their geological and geomorphological features are suggestive of normal or oblique faulting (Elitez and Yaltırak, 2023). The major faults offset the basement rocks in the northern, south-western, and easternmost parts of the Eşen Basin. In the central and southern areas where the Neogene sediments are dominant, the major faults locally juxtapose the basement rocks against the Neogene lacustrine sediments and the Quaternary alluvial deposits (Figures 2 and 4).

3. Materials and methods

This paper describes the geological and geomorphological properties of the Eşen Basin based on both classical and recent methods. The geological, rock strength and fault maps used as sources have been produced using a database by integrating a digital elevation model (DEM), high-resolution satellite images, multibeam bathymetric map, and field studies describing exact formation contacts and fault relationships. Although geological mapping is one of the most important aspects of geoscience research, digital elevation models and satellite images are also efficient and effective ways of revealing geomorphological features. The interpretation of the tectonic setting of a region is greatly facilitated by the integration of classical field techniques with digital technologies. In this context, a digital elevation model and a geological map of the Eşen River Basin at a scale of 1:25,000 were produced. These were superimposed on noncommercial Google Earth satellite images using the Geographic Information System (GIS) software product ESRI ArcGIS Desktop 10.4.1® for examining morphotectonic features and calculating geomorphic indices. Additionally, some of the numerical data such as k_{sn} values and knickpoints were analysed using Matlab-based Topo-Toolbox (Schwanghart and Scherler, 2014). The 30 m-resolution data collected by the Turkish Navy, Department of Navigation, Hydrography and Oceanography and the 250 m-resolution EMODNET (European Marine Observation and Data Network, Portal for Bathymetry; https://www.emodnet-bathymetry.eu/) data were integrated to produce a multibeam bathymetric map (GeoTIFF) including the coast and nearshore areas.

In this study, the 101 subbasins were manually delineated using a digital elevation model (Figure 6). The analysis of the geomorphic indices is useful to validate the geomorphic developments related to active tectonics

Figure 5. Several major faults observed in the study area. (a) Ören Fault (coordinates 36°46′2.88″N, 29°24′31.30″E), (b) Yakaköy Fault (coordinates 36°32′57.93″N, 29°27′0.62″E). Red arrow indicates an example of a knickpoint, (c) a normal fault juxtaposing Cretaceous neritic limestones and lower Miocene limestones (Fault 24 in Figure 2; coordinates 36°28′39.98″N, 29°26′18.34″E), (d) Karaköy Fault (coordinates 36°22′56.81″N, 29°17′57.17″E), (e) northern section of the Yakaköy Fault (coordinates 36°39′3.12″N 29°29′7.44″E), (f) a left lateral oblique normal fault (Fault 35 in Figure 2; coordinates 36°39′1.56″N, 29°29′34.32″E), (g) Saklıkent Fault (coordinates 36°29′46.04″N, 29°25′6.02″E), (h) a normal fault juxtaposing Mesozoic limestones and alluvial sediments (Fault 35 in Figure 2; coordinates 36°22′56.52″, 29°19′8.10″E).

(Bull and McFadden, 1977; Keller and Pinter, 2002). The drainage basin asymmetry factor (AF; Hare and Gardner, 1985; Cox, 1994), transverse topography symmetry factor (T; Cox, 1994), basin shape index (Bs; Ramírez-Herrera, 1998), hypsometric curves and hypsometric integral (HI; Strahler, 1952), valley-floor width to valley height ratio (Vf; Bull and McFadden, 1977; Bull, 1977, 1978), mountain front sinuosity ratio (Smf; Bull and McFadden, 1977; Bull, 1977, 1978), stream length gradient index (SL; Keller and Pinter, 2002), and normalized channel steepness index (k_{sn}; Wobus et al., 2006) were used to analyse the relative tectonic activity index (Iat; El Hamdouni et al., 2008) according to the analytical hierarchy process (AHP) method (Saaty, 1977).

3.1. Drainage basin asymmetry factor (AF)

The drainage basin asymmetry factor (AF) can be used to detect tectonic tilting of a drainage basin (Hare and Gardner, 1985). AF = 100 × (Ar / At) where Ar is the area of the drainage to the right of the trunk stream looking

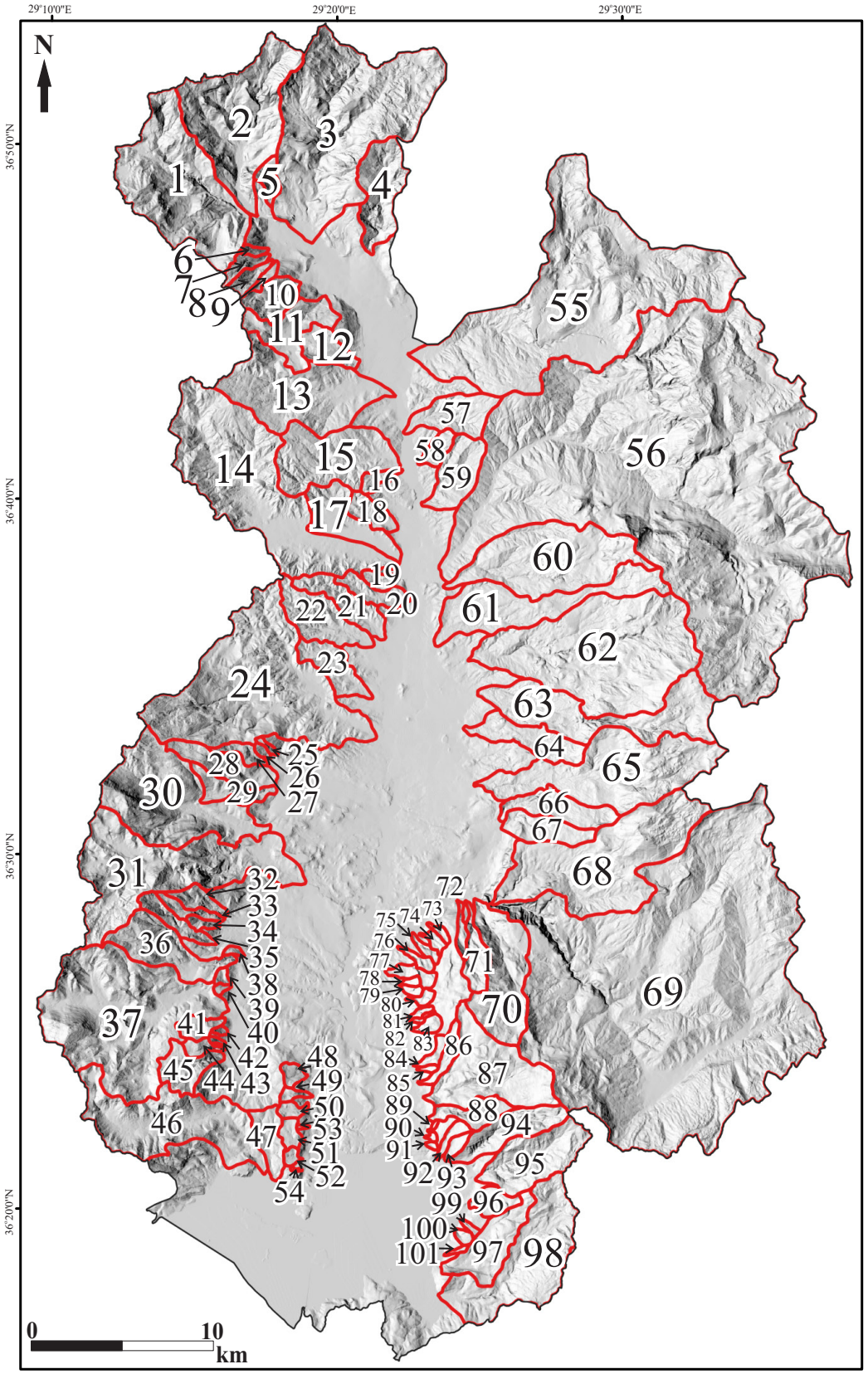

Figure 6. Digital elevation model of the Eşen Basin showing locations of the drainage basins.

downstream and At is the total area of the drainage basin (Keller and Pinter, 2002). For a stable setting, the AF value should equal about 50. This situation represents a symmetric basin. The AF value greater than or less than 50 indicates basin tilting as a result of tectonic activity. To describe the asymmetry levels of the drainage basins, AF' = |AF-50| equation is used. AF' > 15, AF' = 7–15, and AF' < 7 indicate strongly asymmetrical basins, moderately asymmetrical basins, and symmetrical basins, respectively (El Hamdouni et al., 2008).

3.2. Transverse topography symmetry factor (T)

The transverse topographic symmetry actor (T) is used to evaluate the tilting of a basin due to the presence of tectonic activity. T is determined by analysis of the basin symmetry vector data, which includes the deflection of the river from the midline of the basin (Cox, 1994). T = (Da / Dd), where Da is the distance from the river channel to the middle of its drainage basin and Dd is the distance from the midline of the drainage basin to the basin divide. The T factor ranging from 0 to 1 indicates perfectly symmetric to asymmetrical basins (Cox, 1994; Keller and Pinter, 2002).

3.3. Basin shape index (Bs)

Basin shape index (Bs) is defined as Bs = Bl / Bw, where Bl is the length between the highest point and the mouth of a basin and Bw is the width at the widest point of a basin. The lower Bs values tend to be circular in shape indicating lower tectonic activity. Rapidly uplifted mountain fronts generally produce steep and much more elongated basins (Bull and McFadden, 1977; Ramírez-Herrera, 1998). Bs values are categorized into three classes: high tectonic activity with Bs > 1.76, moderate tectonic activity with 1.11 ≤ Bs ≤ 1.76, and low tectonic activity with Bs < 1.11 (Sharma et al., 2018).

3.4. Hypsometric curves and hypsometric integral (HI)

Hypsometric curves and hypsometric integral (HI) are generally used to evaluate the state of geomorphic evolution of a drainage basin (Willgoose and Hancock, 1998; Guarnieri and Pirrotta, 2008; Pérez-Peña et al., 2010). The shape of a hypsometric curve (Willgoose and Hancock, 1998) is directly associated with the distribution of basin area and elevation and can indicate the relative age of the basin. While convex shape basins represent the young stage, concave and S-shaped curves denote old and mature stages, respectively (Hack, 1973). In addition to these curves, the hypsometric integral (HI) gives a clue about the degree of erosion (Strahler, 1952). High values of the hypsometric integral with convex curves are possibly related to young tectonic activity and indicate severe erosion. Low values with concave curves reflect little erosion and old tectonic activity. The formula for Hi is defined as; HI = (Hmean – Hmin) / (Hmax – Hmin) (Pike and Wilson, 1971). Here, Hmean, Hmin, and Hmax are the average, minimum, and maximum elevations of the drainage basin, respectively.

3.5. Valley-floor width to valley height ratio (Vf)

The valley-floor width to valley height ratio (Vf) (Bull and McFadden, 1977; Bull, 1977, 1978) is another analysis showing whether a basin has a V-shaped or a U-shaped valley. Vf is calculated as 2Vfw / [(Eld - Esc) + (Erd - Esc)]. Here, Vfw is the width of the valley floor, Esc is the elevation of the valley floor and Eld and Erd are the elevations of the left and right valley divides, respectively. If the basin has been strongly uplifted, the Vf values tend to be smaller (Vf < 1), resulting a V-shaped valley. High values of Vf (Vf > 1) represent relatively low uplift rates with U-shaped valleys. Then Vf values are classified into three classes: high tectonic activity with Vf < 0.5, moderate tectonic activity with 0.5 ≤ Vf ≤ 1 and low tectonic activity with Vf > 1 (El Hamdouni et al., 2008).

3.6. Mountain-front sinuosity index (Smf)

Mountain-front sinuosity index (Smf) (Bull and McFadden, 1977; Bull, 1977, 1978) signifies the balance between erosional forces and tectonic forces. Smf is defined as Lmf / Ls, where Lmf is the length of the mountain front along the foot of the mountain, at the pronounced break of the slope and Ls is the straight-line length of the mountain front. On the most tectonically active fronts, Smf values approach 1 and may increase to 1.4 (Rockwell et al., 1985; Keller, 1986). For slightly active regions, the Smf values range between 1.4 and 3. In this study, Smf values are classified into high tectonic activity with Smf < 1.1, moderate tectonic activity with 1.1 ≤ Smf < 1.5, and low tectonic activity with Smf ≥ 1.5. (El Hamdouni et al., 2008).

3.7. Longitudinal river profiles and stream length gradient index (SL)

A longitudinal river profile is a cross-sectional pilot representing the elevation differences between the headwaters and the mouth of a river (Keller and Pinter, 2002). Longitudinal river profiles with SL index values are used to describe the changes and irregularities on lithological, structural, and tectonic processes dominating the area (Hack, 1973; Bull, 2008). Stream length gradient index (SL) indicates the stream power, which is a good predictor of channel erosion. The SL index also reflects the relationship between tectonic uplift, rock resistance, and topography (Keller, 1977; Merritts and Vincent, 1989; Font et al., 2010). The index decreases where the river crosses the relatively soft rocks and increases on relatively hard rocks. If there is an inconsistency, then the SL index may represent tectonic activity. SL = (ΔH / ΔL) / L, where ΔH is the difference in height between two points, ΔL is the difference in length between two points, and L is the total

length of the river (Hack 1973). To detect local responses to regional processes such as regional uplift (Troiani and Della Seta, 2008), both a map of SL distribution along the rivers and rock strength levels (ISRM, 1978; Marinos and Hoek, 2001) and an SL density map were produced for this study. SL density map was generated using the Kernel density tool of ArcGIS with a search radius of 1500 m and an output cell size of 20 m^2.

The longitudinal river profiles with the stream length gradient index (SL) values represent the erosion-sedimentation equilibrium or steady-state position of the rivers. Sudden changes in stream slope are defined by SL index values and indicate the topographic or lithological breaks.

3.8. Knickpoints and normalized channel steepness index (k_{sn})

A knickpoint in river systems is characterized as a sharply inclined section situated between areas of lower gradient along the course of the river (Howard et al., 1994). Knickpoints represent distinct changes in the steepness of river profiles, and their characteristics and behaviour are influenced by both the nature of the perturbation and the mechanics of river incision (Kirby and Whipple, 2012). They can be caused by a resistant lithology, an increase in shear stress, or surface uplift (Bishop et al., 2005). They can be observed at lithological boundaries, particularly where a harder and more durable layer overlies a softer and more erodible layer.

The evaluation of stream profiles in the study area is based on Flint's empirical power-law equation, which relates the local slope (S) to the upstream contributing drainage basin area (A): $S = k_s A^{-\theta}$, where k_s is a channel steepness index and θ is the concavity index. k_s, as an important metric for geomorphological studies, exhibits sensitivity to spatial variations in bedrock erodibility, climate, and uplift rate. Increased values of k_s may be associated with abnormal uplift rates or a more general decrease in erodibility (Snyder et al., 2000; Kirby and Whipple, 2001). The concavity index, θ, is a measure of the rate at which the gradient of a river channel decreases as it moves downstream. To compare k_s within different channels, it is common to calculate the steepness index with a fixed value of θ. This value is referred to as the reference concavity index, θ_{ref}. Whenever a reference concavity index is used, the obtained value of the channel steepness index is called 'normalized' and is represented by k_{sn} with fixed units (Wobus et al., 2006). Recent studies (e.g., Snyder et al., 2000; Kirby and Whipple, 2001; Wobus et al., 2006) suggest that the steepness index is dependent on uplift rate, and also theoretical considerations, in line with empirical data, indicate that, under steady-state conditions, the θ value is expected to be between 0.4 and 0.6, with a best-fit value of 0.45 (Tarboton et al., 1989; Whipple and Tucker, 1999; Snyder et al., 2000; Kirby and Whipple, 2001; Kirby et al., 2003; Lague and Davy, 2003; Whipple, 2004; Wobus et al., 2006). Therefore, a reference concavity of 0.45, which means that the dimension of k_{sn} is $m^{0.9}$ ($m^{2\theta}$), is used in this study.

There are two types of knickpoint recognised in the literature: vertical-step and slope-break (Wobus et al., 2006; Kirby and Whipple, 2012). The vertical-step knickpoints suggest no obvious change in k_{sn} values, whereas the slope-break knickpoints show upstream and downstream segments with different k_{sn} values. Slope-break knickpoints are crucial for the interpretation of tectonic activity in erosional landscapes (Wobus et al., 2006).

Rivers with higher k_{sn} values reflect higher uplift rates in regions with similar climate and rock strength, as well as high erosion rates and steep slopes, whereas those with lower k_{sn} values characterise the low uplift zone (Synder et al., 2000; Wobus et al., 2006; Kirby and Whipple, 2012). Locally, k_{sn} values may exhibit knickpoints even in the absence of a fault or lithological changes. This scenario may suggest a potential tectonic origin (Ouayah et al., 2021) or be attributed to erosion processes (Kirby and Whipple, 2012).

3.9. Relative tectonic activity (Iat) and analytical hierarchy process (AHP)

The relative tectonic activity (Iat) is a strong method to combine geomorphic indices and reflect the differences in the tectonic activity in a region (Keller and Pinter, 2002; El Hamdouni et al., 2008). The geomorphic indices are averaged (S/n) and divided into four classes: very high with $1 \leq Iat < 1.5$ (class 1); high with $1.5 \leq Iat < 2.0$ (class 2); moderate with $2 \leq Iat < 2.5$ (class 3), and low with $2.5 \leq Iat$ (class 4) (El Hamdouni et al., 2008). In this study, Iat was analysed according to the analytical hierarchy process (AHP) method. The AHP method is used to classify the indices based on their intensity of importance: 1 for equal importance, 3 for moderate importance, 5 for strong or essential importance, 7 for very strong importance, 9 for extreme importance, and 2, 4, 6, 8 for intermediate values (Saaty, 1977). The Cr coefficient must be ≤0.1.

4. Results

4.1. Drainage basin asymmetry factor (AF)

To evaluate the tectonic tilting of the Eşen Basin, the drainage basin asymmetry factor (AF) values of the 101 drainage basins were calculated. The calculated AF and AF' results are shown in Figure 7a and Table 1. The AF values of the drainage basins range from 14.35 to 85.84 and the AF' values range from 0.02 to 35.84 (Table 1). Approximately 35% (35/101) of the AF' results have values of >15 and indicate strongly asymmetrical basins. Approximately 27% (27/101) of the values ranging between 7 and 15 represent moderately asymmetric features, and approximately 39%

(39/101) of the drainage basins are symmetric (Figure 7a). As far as their tilting direction is concerned, 16 drainage basins are north-westward tilted, 8 are north-eastward tilted, 11 are northward tilted, 16 are south-westward tilted, 8 are south-eastward tilted, 1 are southward tilted, and the remaining 1 is westward tilted. In brief, the drainage basins are differentially tilted in different directions due to continuous tectonism within the basin (Figure 7a).

4.2 Transverse topography symmetry factor (T)

T was calculated at a distance interval of 200 m and then an average value was obtained for each drainage basin. The average T values are classified into tree classes: Class 1 (≥0.5), Class 2 (0.5–0.3), and Class 3 (≤0.3) from high to low tectonic activity (Taesiri et al., 2020; Figure 7b). The minimum average value of T obtained in the present study is 0 for basins 53 and 54, and the maximum mean value of T is 0.88 for Basin 17 (Table 1). According to the T values, approximately 19% (19/101) of the drainage basins indicate strongly asymmetrical basins, approximately 30% (30/101) of the T values represent moderately asymmetric features, and approximately 52% (52/101) of the drainage basins are symmetric (Figure 7b).

4.3. Basin shape index (Bs)

The basin shape indexes of the 101 drainage basins range from 0.64 to 5.81 (Table 1). Basin 69 has the lowest value of Bs, while basin 33 has the highest value of Bs, reflecting higher tectonic activity. Most of the basins have an elongated shape indicating tectonic activity. These drainage basins are predominantly observed in the central part of the Eşen Basin (Figure 7c).

4.4. Hypsometric curves and hypsometric integral (HI)

In this study, based on hypsometric curves and hypsometric integral (HI), the drainage basins are divided into three stages: old (HI < 0.3), mature (0.3 ≤ HI ≤ 0.5), and young (HI > 0.5). The HI values of the drainage basins of the Eşen Basin range from 0.25 to 0.80 (Table 1) and 50 of them indicate the young stage (Figure 7d). The other basins reflect relatively long-term erosion. The HI values are not directly related to relative tectonic activity, but they can provide important clues about the amount of erosion and the relative age of landscape (El Hamdouni et al., 2008). For example, the drainage Basin 69 has moderate HI and AF' values and low Bs and T values, despite the low Vf values along three major faults located in and in front of this drainage basin (Figure 8a). This is most likely due to the rugged Western Taurides with high elevation sources of the Eşen River, which generate flash floods after intense rainstorms and during snow-melt periods (Aksu et al., 2021).

4.5. Valley-floor width to valley height ratio (Vf)

The valley-floor width to valley height ratio (Vf) indices were calculated at distances ranging from 100 to 500 m according to the size of the drainage basins. Average Vf values (Vf_{avg}) were calculated for each drainage basin. Vf_{avg} values in the Eşen Basin vary from 0.07 (Basin 3) to 8.79 (Basin 17) (Table 1). Higher Vf values suggest the existence of U-shaped valleys and indicate relatively stable tectonic activity. These drainage basins are predominantly located in the central part of the Eşen Basin. Conversely, lower Vf values along the major faults (Figure 8a) suggest the existence of V-shaped valleys with high degrees of tectonic uplift.

4.6. Mountain-front sinuosity index (Smf)

The mountain front sinuosity index (Smf) is an important tectonic indicator of a region. Calculated Smf values of 41 mountain front lineaments (Figure 8b) in the Eşen Basin vary from 1.0178 to 1.6571 (Table 2). Almost all values reflect an effective tectonic activity in the region. As in Table 2, the most active front fault is Fault 35 with an Smf value of 1.0178 (Figures 5h and 8b). Pliocene to Quaternary alluvial fan and talus deposits along the foot of the N-S- and NE-SW-striking mountain fronts 21, 22, 23, 30, 31, 33, 35, 37, 38, and 39 indicate recent active tectonics. The W-E and NW-SE-striking mountain fronts in the northern section of the basin have developed in the basement rocks (e.g. 15, 16, 17, 18). Some of the river channels display left-lateral displacements (e.g. 20, 23, 27, 30, 31). Additionally, a comparison between Smf values and earthquake locations in the whole basin displays compatibility (Figure 8b).

4.7. Longitudinal river profiles and stream length gradient index (SL)

To identify the factors influencing changes in the SL index, a rock strength level map was produced using the rock classification (Figure 9a). The strength levels R0, R1, R2, R3, R4, R5, and R6 represent extremely weak, very weak, weak, medium strong, strong, very strong, and extremely strong rocks, respectively (ISRM 1978; Marinos and Hoek, 2001). The SL index values for the Eşen River and its tributaries range from 0.4 (Basin 12) to 17051 (on the footwall of the Ören Fault in Basin 55). The analysis reveals that the highest values, signifying anomalies, are widely distributed throughout the eastern section of the basin (Figure 9). When compared with the Vf values, it is noteworthy that the low SL values in most of the drainage basins point out wide and flat river valleys. The different rock types along the river valleys tend to influence the SL index values. In conclusion, considering the longitudinal river profiles and the SL index values together, it is evident that the majority of the SL anomalies are closely associated with major faults rather than lithological changes on both sides of the Eşen Basin (Figures 9 and 10).

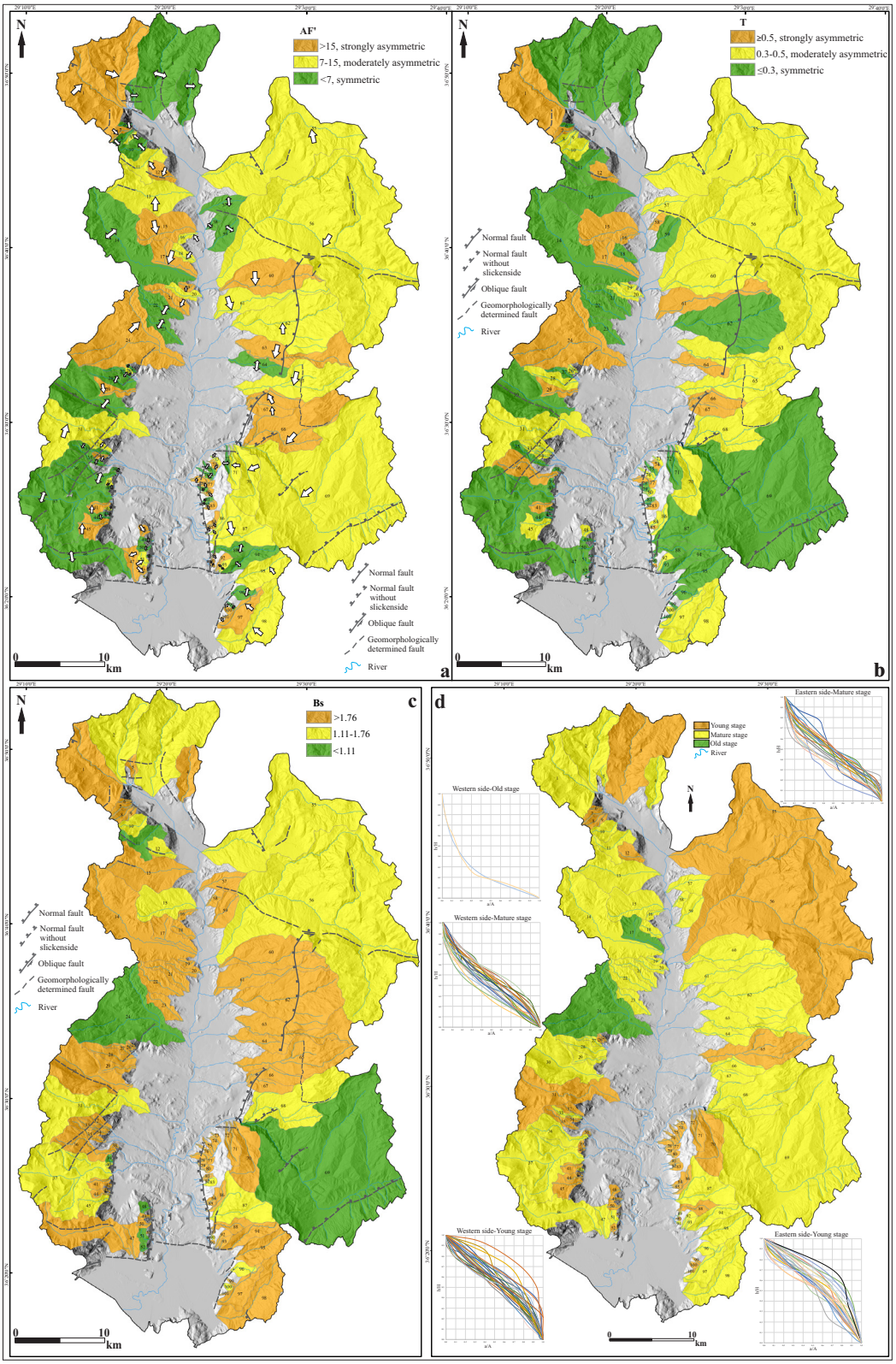

Figure 7. (a) Drainage basin asymmetry (AF'; White arrows indicate tilting directions.), (b) Transverse topography symmetry factor (T), (c) basin shape index (Bs) and (d) stage map based on the hypsometric integral values (HI) and hypsometric curves of the 101 drainage basins of the Eşen Basin.

Table 1. Morphometric values obtained from 101 drainage basins (AF': asymmetry level; T: transverse topography symmetry factor; Bs: drainage basin asymmetry factor; HI: hypsometric integral; Vf_{avg}: average value of valley-floor width to valley height ratio; σ_{n-1}: standard deviation of Vf_{avg} values).

Basin no.	Total area (m^2)	AF'	T	Bs	HI	Vf_{avg}	σ_{n-1}
1	34629769.40	74.51	0.70	1.95	0.39	0.24	0.29
2	30030305.36	69.29	0.22	1.49	0.45	0.38	0.32
3	55774961.91	43.91	0.20	1.39	0.51	0.07	0.03
4	10617674.13	56.95	0.25	2.53	0.47	0.14	0.06
5	1907620.50	46.31	0.27	2.27	0.49	0.55	0.61
6	591478.09	48.79	0.25	2.24	0.56	0.44	0.34
7	1729905.51	27.91	0.51	3.08	0.58	0.33	0.28
8	1793671.21	50.02	0.31	2.82	0.52	0.47	0.06
9	805812.80	58.91	0.47	3.82	0.57	0.69	0.41
10	4769120.69	48.95	0.32	1.46	0.48	0.20	0.12
11	8467032.60	61.30	0.16	1.00	0.47	1.38	2.28
12	4271307.41	31.30	0.55	1.66	0.61	0.33	0.17
13	24751161.77	57.69	0.27	2.34	0.34	1.87	3.09
14	46173938.56	51.59	0.17	2.78	0.35	1.22	0.02
15	16932159.39	23.98	0.58	1.62	0.39	0.19	0.03
16	1435593.29	61.49	0.40	2.28	0.40	1.93	1.97
17	8595035.91	14.35	0.88	2.14	0.25	8.79	0.14
18	3019544.28	38.69	0.09	2.42	0.31	1.92	1.87
19	1353396.45	65.24	0.43	1.91	0.44	0.72	0.00
20	3293114.33	40.07	0.32	3.53	0.38	1.40	0.44
21	5981238.99	34.23	0.07	3.98	0.41	0.94	0.92
22	8845548.22	48.93	0.12	2.35	0.45	2.59	3.35
23	5635379.88	55.82	0.02	3.05	0.33	1.17	0.80
24	51883116.23	85.84	0.73	0.95	0.25	0.35	0.12
25	380970.58	49.09	0.24	3.80	0.62	0.23	0.00
26	432921.92	63.02	0.37	2.12	0.58	0.24	0.00
27	1690035.87	54.93	0.16	2.87	0.46	0.64	0.26
28	6588439.11	43.36	0.31	3.25	0.45	0.40	0.32
29	3892985.62	32.85	0.56	2.07	0.43	0.41	0.08
30	27820179.20	54.12	0.18	1.81	0.41	1.54	2.47
31	35248605.40	58.85	0.33	1.61	0.53	0.27	0.21
32	2431286.32	39.35	0.41	2.38	0.52	0.32	0.23
33	1781858.88	44.41	0.44	5.81	0.50	0.33	0.06
34	846926.05	68.96	0.36	2.02	0.52	0.28	0.00
35	3212060.74	51.57	0.27	4.20	0.50	0.21	0.02
36	10795433.83	53.68	0.50	1.92	0.47	0.38	0.17
37	46950284.98	55.61	0.17	1.30	0.38	2.40	2.74
38	389504.78	44.83	0.18	2.49	0.60	0.27	0.00
39	565077.88	57.08	0.20	0.87	0.57	0.37	0.04
40	352546.77	54.17	0.18	1.67	0.63	0.35	0.06
41	2129858.13	77.95	0.66	1.96	0.63	0.27	0.00
42	276843.67	39.21	0.25	1.81	0.48	0.68	0.56
43	233632.20	52.85	0.07	2.90	0.59	0.73	0.16
44	1308589.46	43.09	0.08	2.37	0.78	0.31	0.21
45	5074331.87	67.03	0.37	1.32	0.57	0.48	0.00
46	25826099.29	51.47	0.28	3.24	0.49	0.65	0.44
47	4314808.96	30.17	0.04	2.35	0.47	0.27	0.12
48	1172882.12	27.49	0.40	1.01	0.60	0.32	0.00
49	747628.28	47.75	0.17	2.05	0.67	0.47	0.00
50	1034646.90	45.93	0.19	1.87	0.68	0.71	0.23
51	1493083.14	57.18	0.17	1.09	0.50	2.59	2.98

Table 1. (Continued.)

52	639482.72	21.01	0.25	0.92	0.57	0.29	0.00
53	117525.94	51.60	0.00	3.21	0.71	1.82	0.00
54	82983.68	57.62	0.00	4.81	0.80	0.60	0.30
55	83382141.90	35.87	0.42	1.63	0.51	0.39	0.19
56	224141023.84	58.38	0.30	1.49	0.51	0.37	0.72
57	7224274.60	43.23	0.34	2.21	0.39	1.71	0.59
58	1932416.18	44.73	0.77	2.05	0.40	1.20	0.83
59	7389895.21	44.49	0.26	1.93	0.38	0.52	0.10
60	25859285.35	69.59	0.33	2.90	0.35	0.72	0.30
61	18573228.43	64.33	0.51	4.37	0.32	1.48	0.63
62	49429086.60	40.65	0.20	1.78	0.45	0.35	0.10
63	22168079.65	79.42	0.47	3.40	0.48	0.65	0.91
64	7431911.37	50.80	0.57	3.94	0.37	0.95	0.06
65	29941083.06	64.93	0.32	2.91	0.51	0.43	0.25
66	6931818.26	23.62	0.56	3.87	0.43	0.63	0.41
67	5561692.18	31.03	0.51	2.29	0.48	1.31	1.69
68	36119592.48	80.28	0.42	1.70	0.49	0.24	0.29
69	188702436.86	60.37	0.25	0.64	0.41	0.70	0.66
70	16101410.97	64.61	0.31	2.63	0.67	0.22	0.10
71	3822004.56	60.31	0.28	3.60	0.62	0.22	0.07
72	1168565.49	54.47	0.28	5.29	0.59	0.80	0.51
73	491925.23	64.05	0.46	3.51	0.55	0.86	0.00
74	779035.99	22.99	0.72	2.21	0.57	2.68	0.46
75	820436.98	48.90	0.28	3.49	0.53	0.27	0.00
76	921527.67	43.51	0.44	2.49	0.61	0.56	0.00
77	1383600.86	25.28	0.58	2.48	0.53	2.09	2.41
78	386219.98	34.27	0.30	2.20	0.54	0.29	0.00
79	514855.57	52.42	0.30	2.10	0.50	0.24	0.08
80	683690.67	32.49	0.37	2.46	0.68	0.56	0.00
81	427213.17	43.59	0.05	2.83	0.54	0.42	0.00
82	286221.28	45.48	0.13	4.82	0.50	0.45	0.00
83	978862.74	23.54	0.55	1.75	0.68	0.31	0.00
84	1123739.51	34.32	0.41	2.76	0.62	0.98	0.00
85	310364.52	23.33	0.66	2.75	0.52	1.39	0.00
86	2056626.54	42.93	0.38	4.64	0.51	0.24	0.00
87	18697781.87	59.43	0.26	1.19	0.46	0.38	0.21
88	4010647.39	53.77	0.23	2.14	0.56	0.18	0.04
89	152761.56	34.66	0.20	3.24	0.49	0.44	0.00
90	210198.77	16.09	0.08	1.23	0.50	2.14	0.00
91	197243.72	72.80	0.56	1.97	0.45	1.68	0.00
92	1175948.13	27.41	0.36	3.28	0.48	0.76	0.00
93	1005313.48	39.75	0.25	2.70	0.42	0.37	0.00
94	7807680.88	44.84	0.29	2.87	0.46	0.32	0.10
95	12518507.59	36.43	0.20	2.51	0.49	0.15	0.11
96	2687150.43	45.69	0.20	1.58	0.47	0.35	0.23
97	9006621.71	20.34	0.48	2.84	0.36	0.34	0.14
98	23830045.17	36.28	0.46	2.73	0.47	0.25	0.23
99	383536.13	45.22	0.05	2.71	0.74	0.38	0.00
100	597906.97	74.12	0.35	1.39	0.61	0.19	0.00
101	281428.96	30.48	0.29	4.27	0.64	1.71	0.00

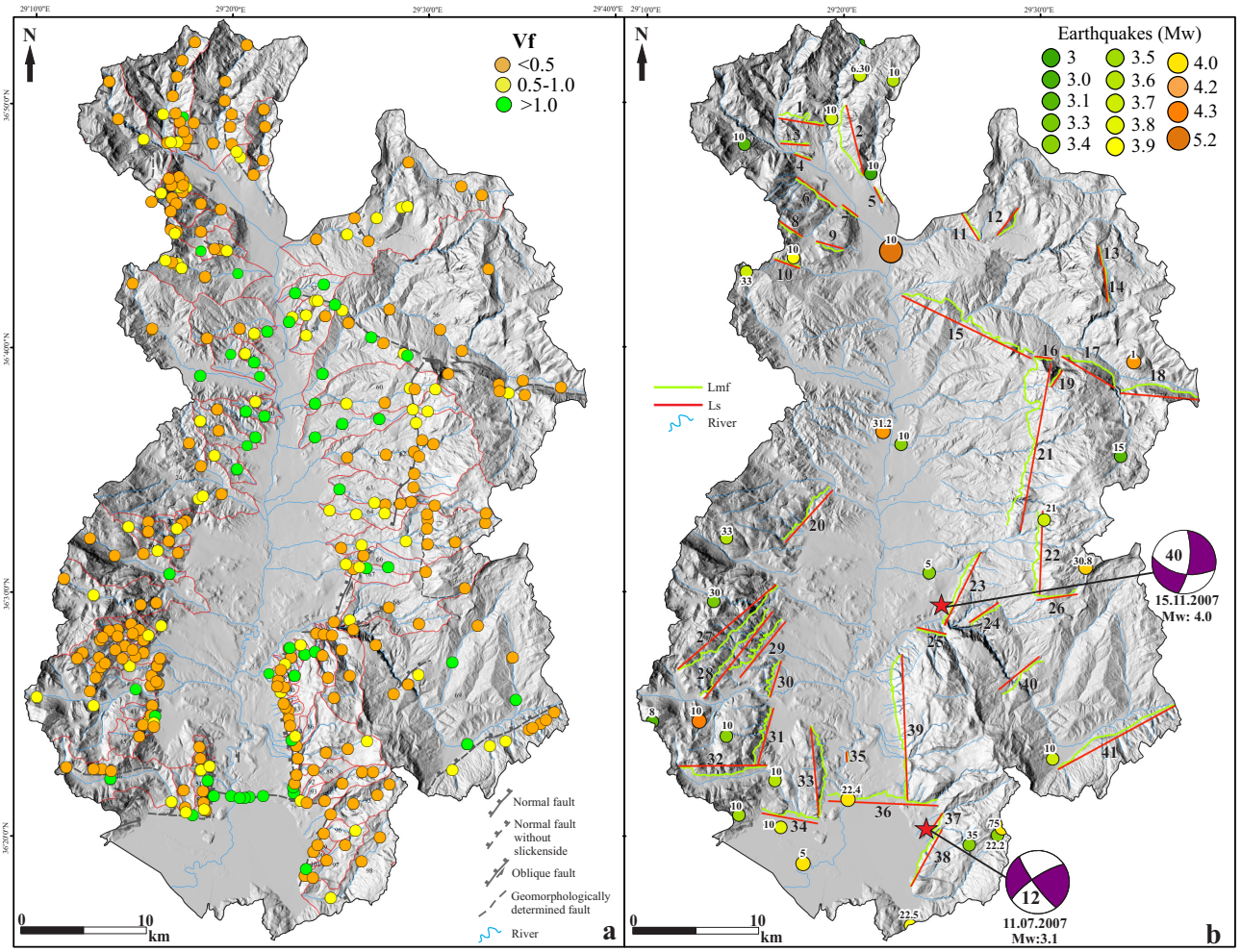

Figure 8. (a) Digital elevation model of the Eşen Basin showing valley width to valley height ratio (Vf) locations, (b) Digital elevation model of the Eşen Basin showing the mountain front numbers, Lmf and Ls lines used for Smf (mountain front sinuosity index) calculations and earthquake data points (with depths in km). Earthquake focal mechanism solutions are shown in purple beach balls with dates and numbers indicating the depths of earthquakes. Earthquake data from Över et al. (2013) and USGS earthquake catalogue (Accessed on 30 November 2023).

Table 2. Values of the Smf (mountain front sinuosity index) in the defined mountain fronts (Lmf: length of the mountain front along the foot of the mountain; Ls: straight-line length of the mountain front).

Mountain front no.	Lmf	Ls	Smf	Inference
1	4837.1348	3394.1119	1.4252	Moderate tectonic activity
2	6073.1770	5384.5910	1.1279	Moderate tectonic activity
3	2226.9169	2100.7359	1.0601	High tectonic activity
4	1270.9267	1234.2327	1.0297	High tectonic activity
5	1362.7869	1299.3519	1.0488	High tectonic activity
6	3901.0280	3670.2115	1.0629	High tectonic activity
7	1458.4005	1420.9040	1.0264	High tectonic activity
8	2322.8806	2019.5359	1.1502	Moderate tectonic activity
9	2270.8877	2076.3196	1.0937	High tectonic activity
10	2021.5313	1939.6506	1.0422	High tectonic activity
11	2612.3967	2407.4701	1.0851	High tectonic activity
12	2800.0225	2573.4946	1.0880	High tectonic activity
13	1490.8857	1453.1563	1.0260	High tectonic activity

Table 2. (Continued.)

14	2652.4438	2596.0566	1.0217	High tectonic activity
15	13482.9417	10772.3274	1.2516	Moderate tectonic activity
16	1385.1375	1264.1351	1.0957	High tectonic activity
17	5269.6873	4551.0641	1.1579	Low tectonic activity
18	6136.4516	5856.4291	1.0478	High tectonic activity
19	1551.7422	1467.5704	1.0574	High tectonic activity
20	6112.7125	5280.7270	1.1576	Moderate tectonic activity
21	16329.8260	12803.3440	1.2754	Moderate tectonic activity
22	7201.9943	6347.6549	1.1346	Moderate tectonic activity
23	6724.3215	6020.5008	1.1169	Moderate tectonic activity
24	2752.5244	2623.5278	1.0492	High tectonic activity
25	2333.8473	2203.3061	1.0592	High tectonic activity
26	3159.4555	3025.6041	1.0442	High tectonic activity
27	10914.5296	9739.5137	1.1206	Moderate tectonic activity
28	9246.1896	8306.9364	1.1131	Moderate tectonic activity
29	8901.6728	5371.9649	1.6571	Low tectonic activity
30	4191.8240	2797.2862	1.4985	Moderate tectonic activity
31	6018.2299	4422.8197	1.3607	Moderate tectonic activity
32	7236.7300	6603.0325	1.0960	High tectonic activity
33	8002.0961	6852.1729	1.1678	Moderate tectonic activity
34	5274.0033	4237.3261	1.2447	Moderate tectonic activity
35	746.1343	733.0722	1.0178	High tectonic activity
36	9647.7597	8195.3214	1.1772	Moderate tectonic activity
37	1985.6996	1861.3644	1.0668	High tectonic activity
38	5338.1345	4842.5708	1.1023	Moderate tectonic activity
39	12739.5398	11115.9304	1.1461	Moderate tectonic activity
40	4216.9118	3894.6290	1.0828	High tectonic activity
41	10317.7507	10073.6427	1.0242	High tectonic activity

4.8. Knickpoints and normalized channel steepness index (k_{sn})

The extracted knickpoints in the Eşen Basin have various drop heights and are distributed over almost all elevations. The numbers of knickpoints from the western and eastern sides of the Eşen Basin are 51 and 96, respectively; however, they are not observed in the western central parts of the basin (Figure 11). The drop heights of the knickpoints range from approximately 30 m to 420 m. Smaller drop heights are generally distributed in the southwestern, northern, and mideastern parts of the basin. The maximum knickpoint drop heights are observed on the footwall of a geomorphologically determined fault (Figure 11; Fault 22 in Figure 2) in the Basin 65 and on the footwall of the Ören Fault in the Basin 55 (Figure 11; Fault 11 in Figure 2).

The obtained normalized channel steepness index (k_{sn}) values indicate a wide range between 0 and 891 $m^{0.9}$ and therefore divided into five groups (Figure 11) in order to reveal the variation clearly. The highest k_{sn} values are 891 $m^{0.9}$ at the Ören Fault in the Basin 55, 617 $m^{0.9}$ in the Basin 3, 559 $m^{0.9}$ in front of the Ören Fault in the Basin 55, 530 $m^{0.9}$ in the Basin 65, and 526 $m^{0.9}$ in the Basin 68. The distribution of k_{sn} values for the major rivers reveals the existence of knickpoints along the rivers in the northern, southwestern, and eastern parts of the Eşen Basin. In addition, these rivers exhibit varying the k_{sn} values (Figure 11).

4.9. Relative tectonic activity (Iat) and analytical hierarchy process (AHP)

The pairwise comparison between AF', T, Bs, Vf_{avg}, HI, Smf, SL, and k_{sn} indices was conducted, and a preference matrix was generated to produce a relative tectonic activity (Iat) map of the Eşen Basin by using ArcGIS AHP 2.0 tool (Figure 10; Marinoni, 2004). The map of SL distribution and rock strength levels (Figure 9) reveals that the majority of the high values of the SL index are within the low resistance rocks and along the major faults. Consequently, the importance of the SL index outweighs that of the other

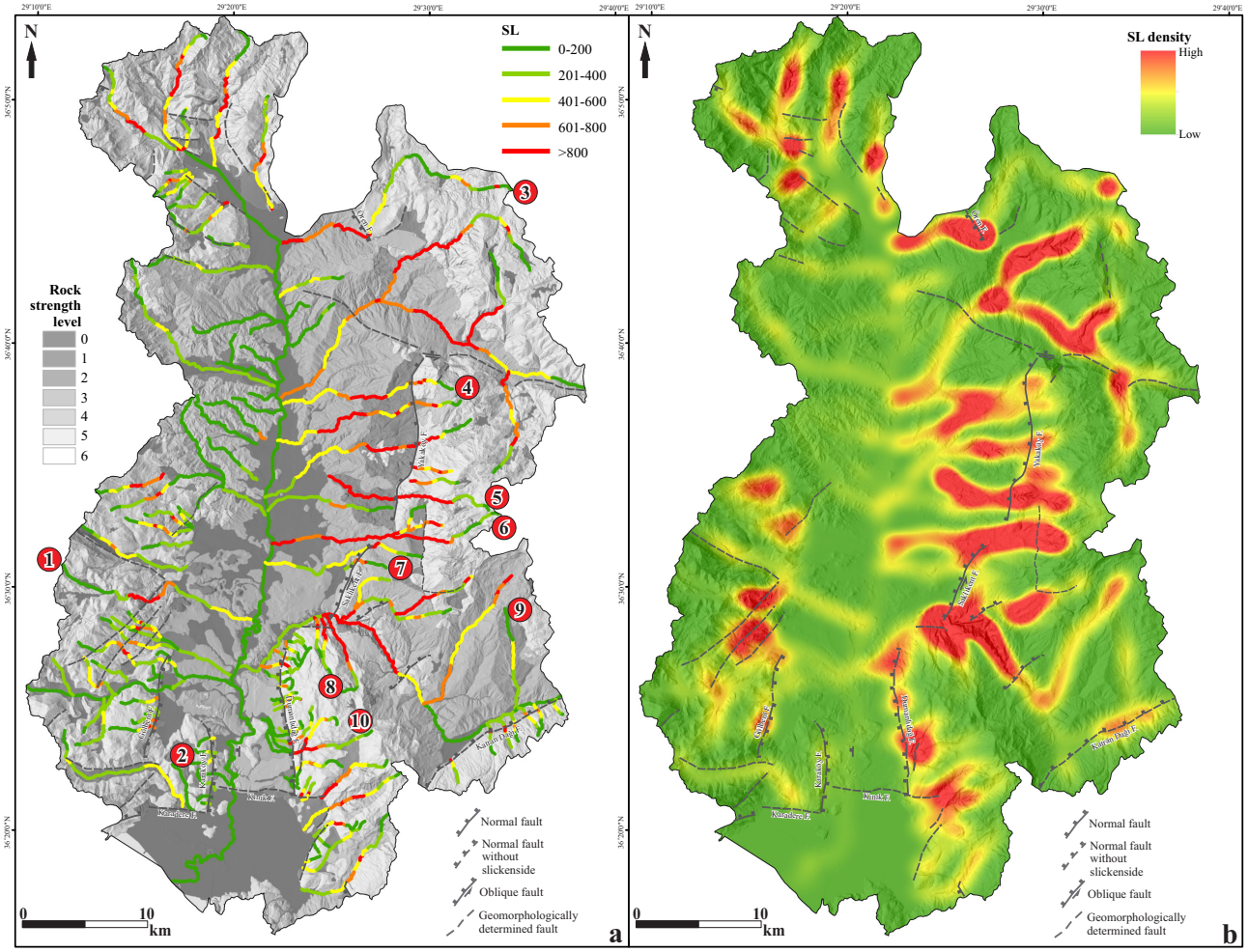

Figure 9. (a) Stream length gradient index (SL) distribution along the main rivers and rock strength levels (ISRM, 1978; Marinos and Hoek, 2001) of the basin rocks. Numbers indicate the longitudinal river profiles in Figure 8. (b) Stream length gradient index (SL) density map.

indices in the preference matrix. Due to its substantial impact on the tectonic activity of drainage basins, k_{sn} also has a higher weight. The HI index is dependent on the rock strength as is the SL index, so that the importance of the HI index is close to that of the SL index. Smf and Vf values are commonly used to calculate uplift rates along tectonically active mountain fronts. In the study area, valleys are predominantly composed of limestone, resulting in a moderate importance of the Vf index in the preference matrix. Mountain fronts are generally straight and represent low values. The importance of the Smf index can be considerably higher than the other indices. However, it is not applicable to all drainage basins, so its importance is ranked after the above indices. The Bs index can vary depending on various effects such as lithology, tectonic setting, and erosion. AF' and T indices display similar behaviour. The AF' index can be an indicator of asymmetry as a function of lithological controls or local climate (Keller and Pinter, 2002). It is particularly effective in areas where drainage basins are parallel to the faults. Similarly, the T index can be influenced by lithology and topographic factors. Consequently, both AF' and T take the lowest values in the matrix (Figure 12).

According to the AHP method, approximately 52.8% of the Eşen Basin (approximately 713.5 km^2) pertains to Class 1; 29.5% (approximately 398.9 km^2) to Class 2; 17.5% (approximately 236.7 km^2) to Class 3; and 0.11% (approximately 1.49 km^2) to Class 4. The eastern and northern parts of the Eşen Basin exhibit very high (Class 1) and high levels (Class 2) of tectonic activity. Especially NE-SW-striking faults (e.g. Dumanlıdağ, Saklıkent, Yakaköy faults) and NW-SE-striking faults of the Gökova-Yeşilüzümlü Fault Zone exhibit very high and high tectonic activities (Figure 13).

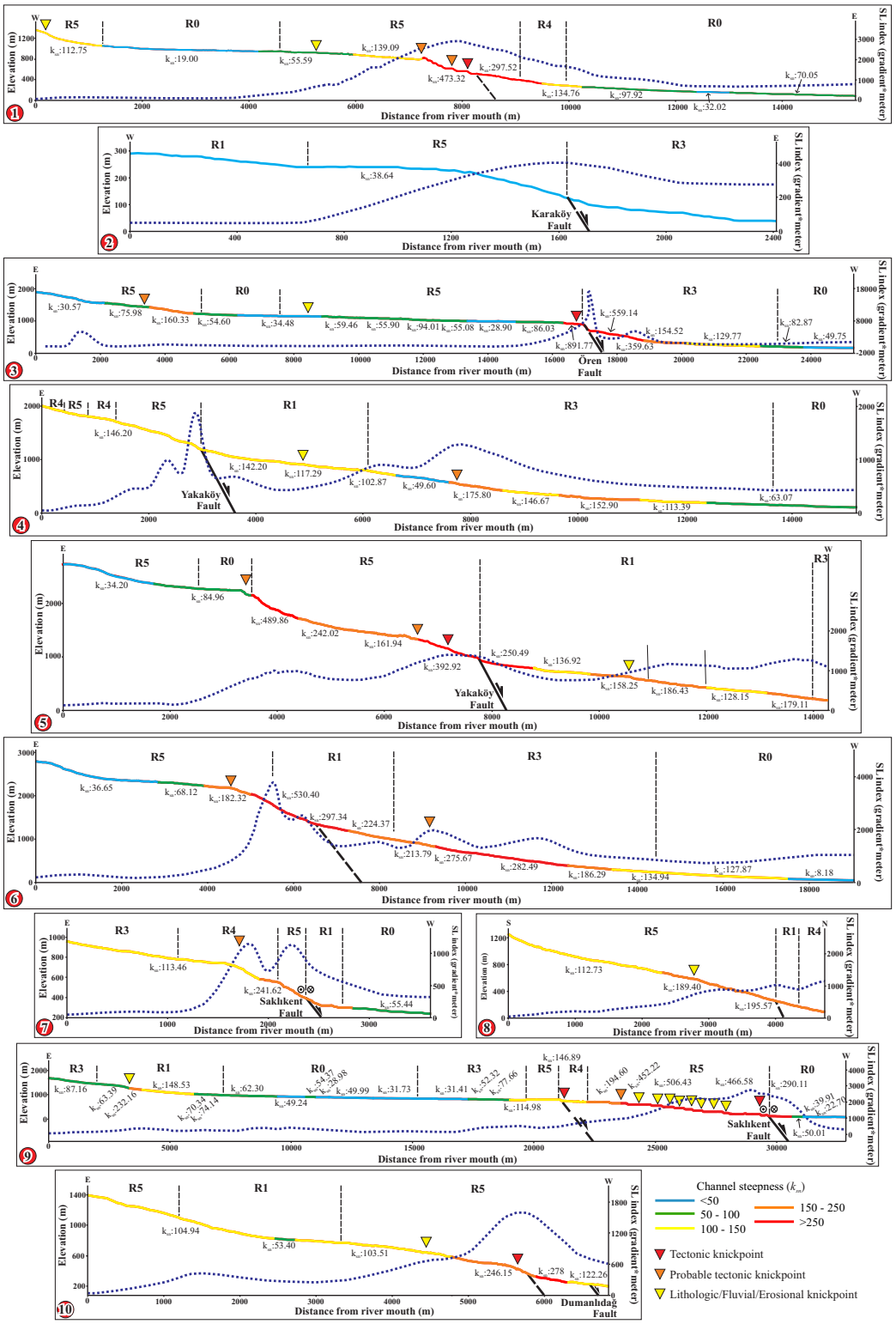

Figure 10. Several longitudinal river profiles of the Eşen Basin with SL profiles, normalized channel steepness index (k_{sn}) values and knickpoints. Location numbers of the rivers are shown in Figure 9a. Blue dotted lines and black dashed lines denote the river SL profile and boundaries between different rock strength levels (R0: extremely weak, R1: very weak, R3: moderately strong R4: strong R5: very strong; Marinos and Hoek, 2001), respectively.

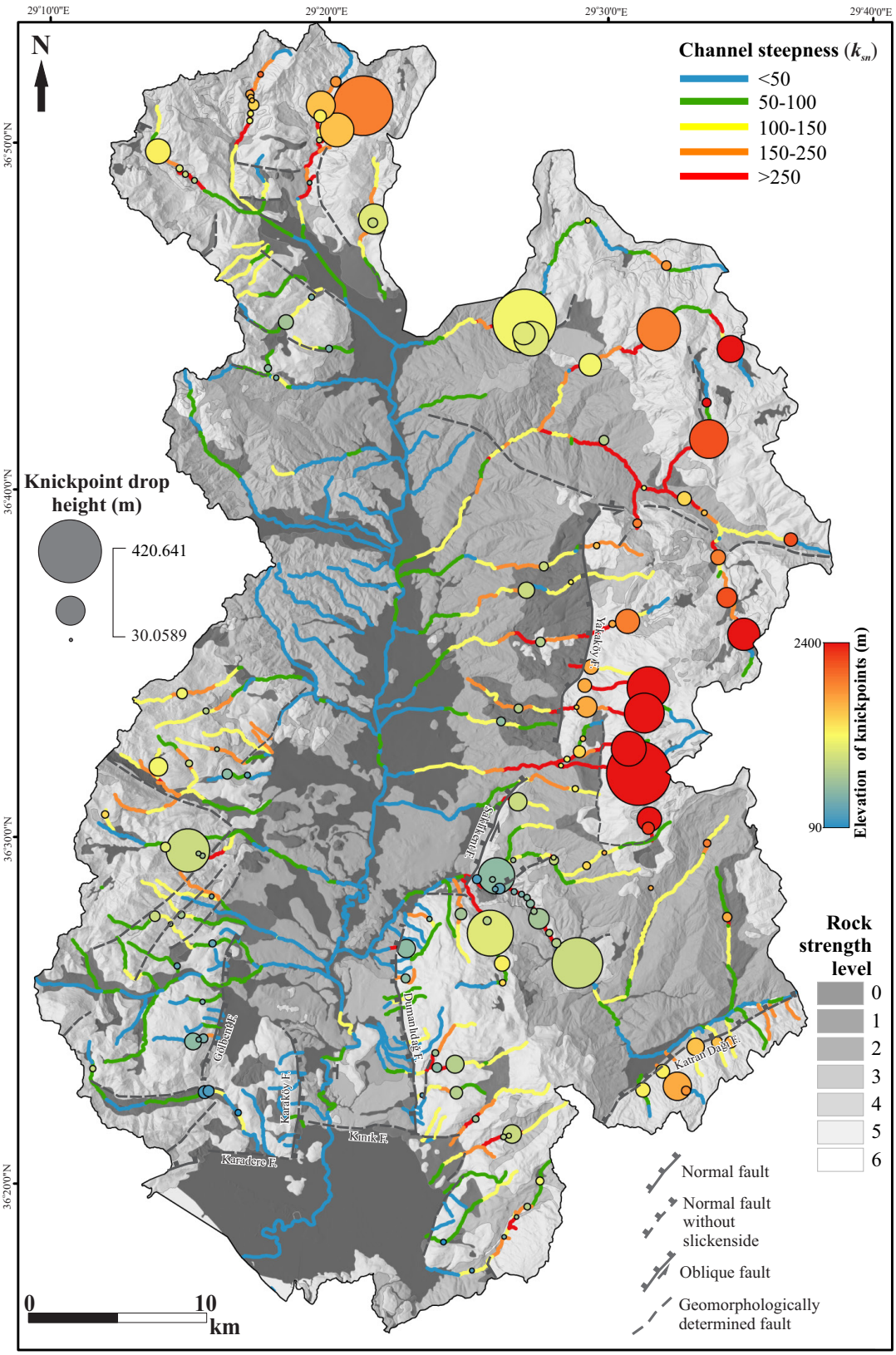

Figure 11. Normalized channel steepness (k_{sn}) distribution along the main rivers and rock strength levels (ISRM, 1978; Marinos and Hoek, 2001) of the basin rocks. Circles indicate the knickpoints.

[Preference matrix]

	AF'	T	Bs	HI	Vf	Smf	SL	Ksn
AF'	1.0	1.0	0.5	0.2	0.25	0.333	0.143	0.143
T	1.0	1.0	0.5	0.2	0.25	0.333	0.143	0.143
Bs	2.0	2.0	1.0	0.4	0.5	2.0	0.286	0.286
HI	5.0	5.0	2.5	1.0	1.25	1.667	0.714	0.714
Vf	4.0	4.0	2.0	0.8	1.0	1.333	0.571	0.571
Smf	3.0	3.0	0.5	0.6	0.75	1.0	2.336	2.336
SL	7.0	7.0	3.5	1.4	1.75	0.428	1.0	1.0
Ksn	7.0	7.0	3.5	1.4	1.75	0.428	1.0	1.0

[Eigenvalues]	[Eigenvector of largest Eigenvalue]	[Criteria weights]	
8.8141	0.0825	AF'	3.2514
-0.4071	0.0825	T	3.2514
-0.4071	0.2301	Bs	9.0725
0.0	0.4124	HI	16.2568
0.0	0.3299	Vf	13.0054
0.0	0.4309	Smf	16.9879
0.0	0.4842	SL	19.0873
0.0	0.4842	Ksn	19.0873

[Consistency ratio CR]
0.0825
(A revision of the preference matrix is recommended if CR > 0.1)

Figure 12. The preference matrix, criteria weights (AF', T, Bs, HI, Vf, Smf, SL, and k_{sn}), and Cr coefficient for classification of relative tectonic activity (Iat).

5. Discussion

This study utilises a comprehensive approach, incorporating both field studies and geomorphic indices, to identify the relationship between active tectonics and geomorphology in the Eşen Basin. In contrast to previous studies that focused primarily on interpreting the local faults and kinematics of the basin, this research recognizes the importance of considering the detailed geological properties of the region. As a tool for understanding tectonic activity in the Eşen Basin, the study focuses on the use of geomorphic indices. The analytical hierarchy process (AHP) is used as a systematic framework for the understanding of the causes of observed tectonic phenomena in the region.

The Eşen Basin is located in the southwestern section of the Burdur-Fethiye Shear Zone, which is bounded by two distinct tectonic regimes: the compressional Western Taurides uplift to the east and the NW-SE extensional system to the west (Elitez et al., 2016; Elitez and Yaltırak, 2016, 2023). GPS-based studies reveal a relative movement between these two regions, indicating the presence of a transtensional system that affects this area (Elitez et al., 2016). Therefore, the Eşen Basin is attributed as a transtensional basin dominantly characterised by N-S- and NE-SW-striking normal and oblique faults associated with the left-lateral shear. On the other hand, the NW-SE-trending normal-oblique Gökova-Yeşilüzümlü Fault Zone, which is located in the northern side of the basin may be considered a contradiction (Figure 2). However, this zone develops parallel to a thrust (Figure 14) due to the uplift of the hanging-wall, which dips to north at an angle of approximately 8° (Hall et al., 2009). The Rhodes Basin is 4 km in depth and the footwall of the Gökova-Yeşilüzümlü Fault Zone indicate a height of approximately 2 km above the sea level. The recent morphological contrast is approximately 6 km. In this case, considering the dip of the thrust, which is 97 km away from the Gökova-Yeşilüzümlü Fault Zone, the zone should link up with the thrust 20 km below. When the earthquakes in the region are analysed, all of the earthquakes along the Gökova-Yeşilüzümlü Fault Zone are shallower than 17 km (Figure 8b) and also located above the thrust block. For example, the largest recorded earthquake is the earthquake of 18 June 1967 in the northern side of the Eşen Basin (Mw 5.2; depth of 10 km; Figure 8b). The fault plane solutions of two earthquakes of 15 November and 11 July 2007 (Mw 4.0 and 3.1, respectively) show a dominant slightly oblique extensional regime. South of the Eşen Basin, the recorded largest offshore earthquake is the earthquake of 14 January 1969 (Mw 6.4). In addition to these earthquakes, the largest onshore and offshore earthquakes occurred around the Eşen Basin since 1925 are the earthquakes of 10 June 2012 (Mw 6; south of Fethiye Bay); 16 August 1925 (Mw 5.6; Yeşilüzümlü); 7 January 1959 (Mw 5.3; Fethiye); and 11 January 1959 (Mw 5.2; Fethiye). The offshore earthquakes are deep with mainly strike-slip and thrust components (Elitez et al., 2016; Elitez and Yaltırak, 2023). Shortly, the Eşen Basin, which is located on the thrusting block, is a NW-SE-extension area in accordance with the direction of the NE-SW compression regime formed in the region where the African Plate subducting beneath the Anatolian Microplate. The Eşen Basin is considered to be within the Burdur-Fethiye Shear Zone. This simply means that NW-SSE and E-W-striking normal faults and fault plane solutions indicating N-S-trending extension can only develop together within a shear zone.

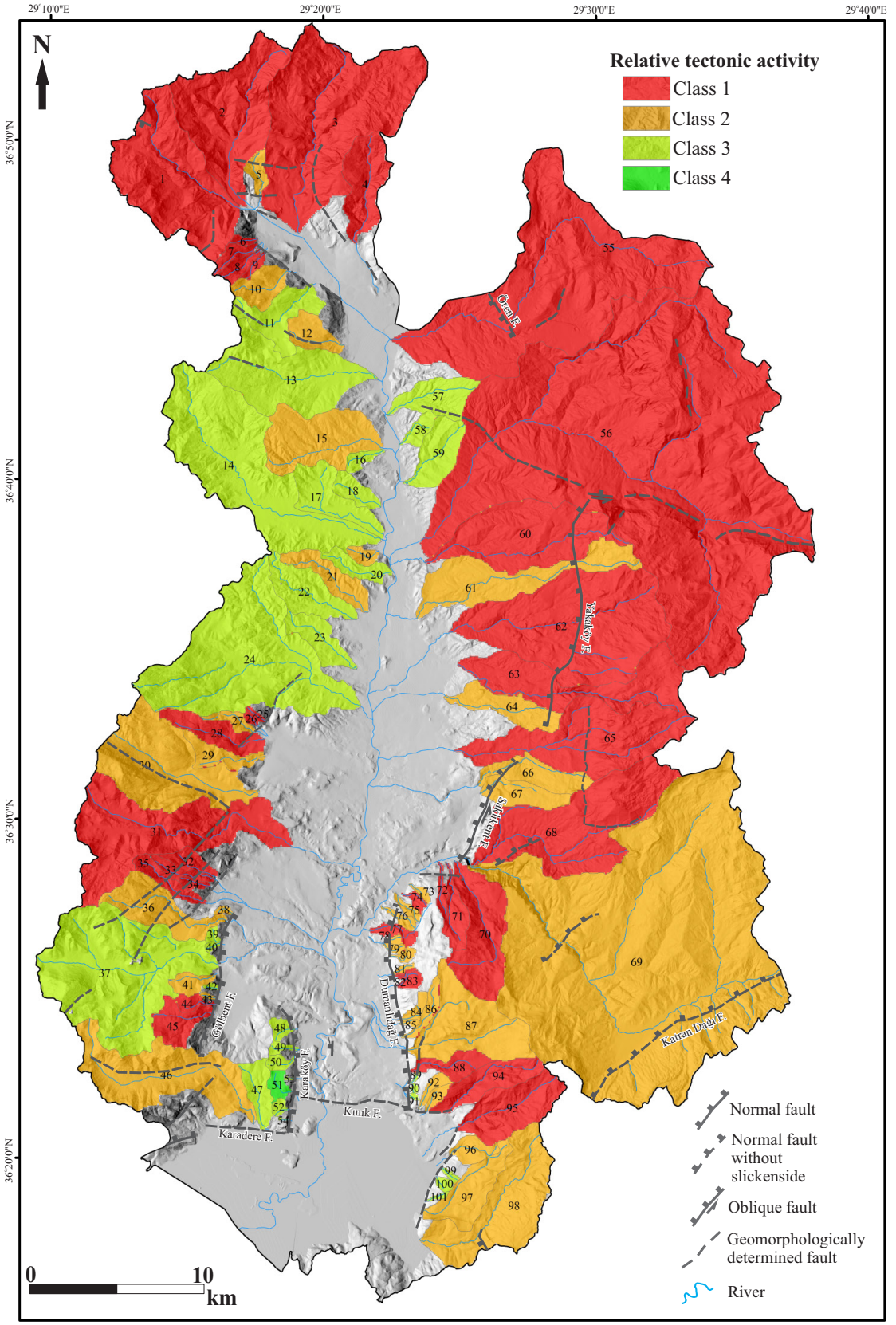

Figure 13. Distribution of relative tectonic activity (Iat) according to the analytical hierarchy process (AHP) method.

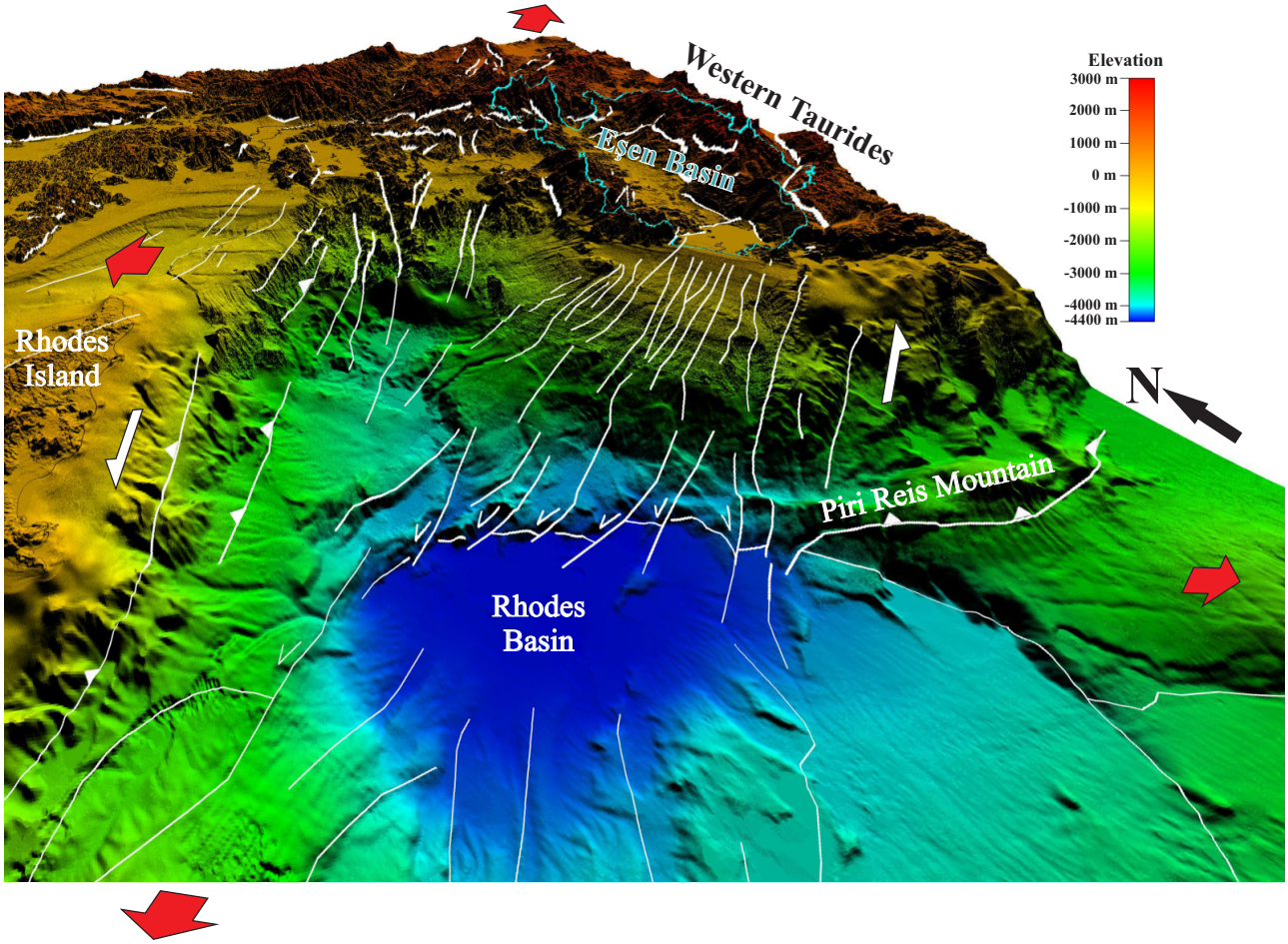

Figure 14. Digital elevation model and multibeam bathymetric map of the study area. White lines show the faults. White arrows show shear direction. Red arrows show the extension directions.

The application of geomorphic indices, including drainage basin asymmetry factor (AF), transverse topography symmetry factor (T), basin shape index (Bs), hypsometric curves and hypsometric integral (HI), valley-floor width to valley height ratio (Vf), mountain front sinuosity index (Smf), stream length gradient index (SL), and normalized channel steepness index (k_{sn}), has proven effective in characterizing the tectonic activity within the Eşen Basin. The distribution of these indices reveals a heterogeneous pattern of tectonic influence across the basin, with distinct variations in asymmetry, transverse topography symmetry, basin shape, and hypsometric characteristics. The prevalence of strongly asymmetrical basins, elongated shapes, and young-stage hypsometric curves collectively suggests ongoing tectonic activity, particularly in the northern and eastern sectors.

The tectonic activity within the basin is not uniformly distributed. Various indices indicate that the northern and eastern parts exhibit a higher level of activity, corroborating the influence of NE-SW-striking faults such as Dumanlıdağ, Saklıkent, and Yakaköy. The NW-SE-striking faults of the Gökova-Yeşilüzümlü Fault Zone also contribute to the observed tectonic features. The spatial variability underscores the complex interplay of different tectonic forces shaping the landscape. The relationship between tectonic activity and major faults is apparent in multiple indices. The anomalies in SL, k_{sn}, and Smf indices highlight the influence of faults on the landscape.

The identification of knickpoints along river profiles provides essential information about abrupt changes in slope and tectonic processes affecting the landscape. The distribution and variation in knickpoint heights indicate differential uplift and fault activity. The association of knickpoints with major faults and the correlation between drop heights and fault locations underscore the significance of tectonic control on landscape evolution. Knickpoints are occasionally observed in rivers that originate from

high-altitude resources (Figure 11). The profiles of these rivers show convexities associated with significant drop heights. Knickpoints are generally located in the limestones with a strength level of R5 and are present in most of the longitudinal river profiles where major faults are present (Figures 10 and 11). However, some of the profiles show sharp knickpoints despite the absence of major faults or resistant rocks (e.g. river profile 5 in Figure 10). This is mainly due to the basement characteristics of the Eşen Basin. Lycian Nappes are composed of many nappes that occurred in different periods. As a result, the basement, which consists mainly of ophiolitic melange and limestones, has a complex composition. This circumstance highlights the importance of considering the existence of old faults in the region.

Regarding the vertical-step knickpoints, there is no obvious variation in k_{sn} values for both upstream and downstream segments; they are associated with differences in the resistivity of geological formations. In contrast, for slope-break knickpoints, the upstream and downstream segments exhibit different k_{sn} values, indicating a tectonic influence (Wobus et al. 2006). k_{sn} values vary within the same rock types in some drainage basins, highlighting the influence of tectonic processes (e.g. profiles 1, 3, 4, 5, 6, 8, 9, 10 in Figure 10). Previous studies have documented similar regions with high uplift rates (e.g. Kirby et al., 2003). Therefore, the observed changes in high k_{sn} values can be interpreted as indicative of the presence of relatively high uplift in these drainage basins.

Analyses of AF', T, Bs, HI, Vf, Smf, SL, and k_{sn} was used to create an index map of the relative tectonic activity (Iat) by using the analytic hierarchy process (AHP). According to the results, most of the geomorphic indices suggest moderate to high tectonic activity (Figure 13). The integration of AHP with the geomorphic indices facilitates a quantitative assessment of relative tectonic activity. The resulting classification into different tectonic classes provides a spatially explicit representation of varying activity levels across the basin. The dominance of Class 1 (very high tectonic activity) in the eastern and northern regions aligns with the observed patterns in geomorphic indices and knickpoint distribution.

The findings of this study contribute valuable information to the broader understanding of the tectonic framework in the region. The correlation between Smf values and earthquake locations, along with the compatibility between k_{sn} values and major faults, strengthens the link between landscape dynamics and regional tectonics. The identification of areas with very high and high tectonic activity has implications for seismic hazard assessment and regional geological studies.

6. Conclusions

This study serves as a valuable contribution to the field of tectonic geomorphology, shedding light on the intricate tectonic dynamics within the Eşen Basin. The combination of geomorphic indices, knickpoints and AHP offers a robust methodology applicable to similar tectonically complex regions, providing a template for further investigations into landscape evolution and tectonic activity. Our field observations and geomorphic analyses lead to the following main conclusion.

- Both sides of the Eşen River are different in terms of morphological characteristics.
- The lithological variations in the basin are not the dominant factor controlling channel steepness. The northern and eastern sides of the Eşen Basin indicate intense tectonic activity. The knickpoints along the longitudinal river profiles generally reflect the response of the tectonic activity in the region. Topographic profiles indicate the uplift in the eastern side of the Eşen Basin. In addition, the elevation difference from north to south on the western side reflects an NW-SE-trending tectonic feature: the Gökova-Yeşilüzümlü Fault Zone.
- The lowest Vf values, observed primarily along major faults, illustrate the presence of narrow and deep valleys, suggesting a high rate of incision associated with tectonic uplift.
- Almost all Smf values display low values representing high tectonic activity and are well-matched with the earthquake locations in the Eşen Basin.
- Abrupt changes in SL values are closely related to the major faults rather than lithological changes in both sides of the Eşen Basin and high SL index values confirm the relative uplift rates in the region.
- High SL and k_{sn} values, indicative of tectonically active regions, are predominantly observed in the northern, eastern, and southwestern parts of the Eşen Basin.
- The various tilting directions of the drainage basins can be evaluated as the effect of the transtensional shear.
- Evaluation of the Iat results obtained by the AHP method suggest that relative tectonic activity in the Eşen Basin is generally high but dominantly very high in the northern and eastern sides. These results indicate better consistency with the tectonic situation of the region.
- The geomorphic indices demonstrating tectonic activity in the Eşen Basin are attributed to the progressive influence of the roll-back of the Hellenic Trench, the compressional region of the Western Taurides and the westward escape of Anatolia since the middle Miocene. These tectonic features control the drainage network pattern.
- In contrast to the studies that deny the presence of the Burdur-Fethiye Shear Zone (e.g. Kaymakçı et al., 2018;

Tosun, et al., 2021), geomorphic indices and topographic features clearly show once again that morphological changes in the Eşen Basin are closely related to the heterogeneous tectonic activity of the Burdur-Fethiye Shear Zone, which has developed under the progressive influence of extension, compression and rotation.

Acknowledgments
The authors are grateful to TÜBİTAK ÇAYDAG (Project No: 107Y005) for financial support to field studies. The authors acknowledge support from the Turkish Naval Forces Office of Navigation, Hydrography and Oceanography (SHOD) and EMODnet (European Marine Observation and Data) for multibeam data. We thank Havva İşkan Işık and Fahri Işık (Akdeniz University) for providing accommodation at the excavation of the ancient city of Patara. We also thank the reviewers and the editor for their helpful contributions to the manuscript.

References

Aksu AE, Hall J, Yaltırak C (2009). Miocene–Recent evolution of Anaximander Mountains and Finike Basin at the junction of Hellenic and Cyprus Arcs, eastern Mediterranean. Marine Geology 258 (1): 24-47. https://doi.org/10.1016/j.margeo.2008.04.008

Aksu AE, Hall J, Yaltırak C, et al. (2014). Late Miocene–Recent evolution of the Finike Basin and its linkages with the Beydağlari complex and the Anaximander Mountains, eastern Mediterranean. Tectonophysics 635: 59-79. https://doi.org/10.1016/j.tecto.2014.04.042

Aksu AE, Hall J, Yaltırak C (2021). Giant slope scars and mass transport deposits across the Rhodes Basin, eastern Mediterranean: Depositional and tectonic processes. Sedimentary Geology 424: 105979. https://doi.org/10.1016/j.sedgeo.2021.105979

Alipoor R, Poorkermani M, Zare M, El Hamdouni R (2011). Active tectonic assessment around Rudbar Lorestan dam site, High Zagros Belt (SW of Iran). Geomorphology 128 (1-2): 1-14. https://doi.org/10.1016/j.geomorph.2010.10.014

Barka A, Reilinger R. (1997). Active tectonics of the Eastern Mediterranean region: deduced from GPS, neotectonic and seismicity data. Annals of Geophysics 40: 587-610.

Bishop P, Hoey TB, Jansen JD, Artza IL (2005). Knickpoint recession rate and catchment area: the case of uplifted rivers in Eastern Scotland. Earth Surface Processes and Landforms: The Journal of the British Geomorphological Research Group 30 (6): 767-778. https://doi.org/10.1002/esp.1191

Brunn JH, de Graciansky PC, Gutnic M, Juteau T, Lefevre R et al. (1970). Structures majeures et corrélations stratigraphiques dans les Taurides occidentales. Bulletin de la Société géologique de France 7 (3): 515-556 (in French).

Bull WB (1977). The alluvial-fan environment. Progress in Physical Geography 1 (2): 222-270.

Bull WB (1978). Geomorphic tectonic classes of the south front of the San Gabriel Mountains, California. U.S. Geological Survey Contract Report, 14-08-001-G-394, Office of Earthquakes, Volcanoes and Engineering, Menlo Park, CA.

Bull W, McFadden L (1977). Tectonic geomorphology north and south of the Garlock Fault, California. In: Doehring DO (Ed.), Geomorphology in Arid Regions, Geomorphology 115-138. https://doi.org/10.4324/9780429299230-5

Cowie PA, Attal M, Tucker GE, Whittaker AC, Naylor M et al. (2006). Investigating the surface process response to fault interaction and linkage using a numerical modelling approach. Basin Research 18 (3): 231-266. https://doi.org/10.1111/j.1365-2117.2006.00298.x

Cox RT (1994). Analysis of drainage-basin symmetry as a rapid technique to identify areas of possible Quaternary tilt-block tectonics: An example from the Mississippi Embayment. Geological Society of America Bulletin 106 (5): 571-581. https://doi.org/10.1130/0016-7606(1994)106<0571:AODBSA>2.3.CO;2

El Hamdouni R, Irigaray C, Fernández T, Chacón J, Keller EA (2008). Assessment of relative active tectonics, southwest border of the Sierra Nevada (southern Spain). Geomorphology 96 (1-2): 150-173. https://doi.org/10.1016/j.geomorph.2007.08.004

Elitez İ, Yaltırak C (2014a). Miocene-Quaternary Geodynamics of Çameli Basin, Burdur-Fethiye Shear Zone (SW Turkey). Geological Bulletin of Turkey 57 (3): 41-67.

Elitez İ, Yaltırak C (2014b). Burdur–Fethiye Shear Zone, Eastern Mediterranean, SW Turkey. Proceedings of EGU General Assembly 2014, Vienna, 16.

Elitez İ, Yaltırak C (2016). Miocene to Quaternary tectonostratigraphic evolution of the middle section of the Burdur-Fethiye Shear Zone, south-western Turkey: Implications for the wide inter-plate shear zones. Tectonophysics 690: 336–354. https://doi.org/10.1016/j.tecto.2016.10.003

Elitez İ, Yaltırak C (2023). Miocene to Quaternary geodynamic evolution of the southern section of the Burdur-Fethiye Shear Zone and its offshore continuation, eastern Mediterranean. Tectonophysics 857: 1-19. https://doi.org/10.1016/j.tecto.2023.229866

Elitez İ, Yaltırak C, Aktuğ B (2016). Extensional and compressional regime driven left-lateral shear in southwestern Anatolia (eastern Mediterranean): The Burdur- Fethiye Shear Zone. Tectonophysics 688: 26–35. https://doi.org/10.1016/j.tecto.2016.09.024

Ersoy E (1990). The analysis of evolution and structural items of the western Taurus-Lycian Nappes. Journal of Geological Engineering 37: 5-16.

Font M, Amorese D, Lagarde JL (2010). DEM and GIS analysis of the stream gradient index to evaluate effects of tectonics: the Normandy intraplate area (NW France). Geomorphology 119 (3-4): 172-180. https://doi.org/10.1016/j.geomorph.2010.03.017

Govers R, Wortel MJR (2005). Lithosphere tearing at STEP faults: response to edges of subduction zones. Earth and Planetary Science Letters 236 (1): 505-523. https://doi.org/10.1016/j.epsl.2005.03.022

Graciansky PC (1972). Recherches géologiques dans le Taurus Lycien occidental. Univ. Paris-Sud (Orsay), PhD Thesis, 731 pp (in French).

Guarnieri P, Pirrotta C (2008). The response of drainage basins to the late Quaternary tectonics in the Sicilian side of the Messina Strait (NE Sicily). Geomorphology 95 (3-4): 260-273. https://doi.org/10.1016/j.geomorph.2007.06.013

Hack JT (1973). Stream-profiles analysis and stream-gradient index. Journal of Research of the US Geological Survey 1 (4): 421-429.

Hall J, Aksu AE, Yaltırak C, Winsor JD (2009). Structural Architecture of the Rhodes Basin: A Deep Depocentre that Evolved since the Pliocene at the Junction of Hellenic and Cyprus Arcs, Eastern Mediterranean. Marine Geology 258: 1-23. https://doi.org/10.1016/j.margeo.2008.02.007

Hall J, Aksu AE, Elitez İ , Yaltırak C, Çifci G (2014). The Fethiye-Burdur Fault Zone: A component of upper plate extension of the subduction transform edge propagator fault linking Hellenic and Cyprus Arcs, Eastern Mediterranean. Tectonophysics 635: 80-99. https://doi.org/10.1016/j.tecto.2014.05.002

Howard AD, Seidl MA, Dietrich WE (1994). Modeling fluvial erosion on regional to continental scales. Journal of Geophysical Research: Solid Earth 99 (B7): 13971-13986. https://doi.org/10.1029/94JB00744

Hare PW, Gardner TW (1985). Geomorphic indicators of vertical neotectonism along converging plate margins, Nicoya Peninsula, Costa Rica. Tectonic geomorphology 4: 75-104.

Huguen C, Mascle J, Chaumillon E, Woodside JM, Benkhelil J et al. (2001). Deformational styles of the eastern Mediterranean Ridge and surroundings from combined swath mapping and seismic reflection profiling. Tectonophysics 343 (1): 21-47. https://doi.org/10.1016/S0040-1951(01)00185-8

ISRM (1978). Suggested Methods for the Quantitative Description of Discontinuities in Rock Masses. International Journal of Rock Mechanics and Mining Science and Geomechanics Abstracts 15: 319-368.

Kaymakçı N, Langereis C, Özkaptan M, Özacar AA, Gülyüz E et al. (2018). Paleomagnetic evidence for upper plate response to a STEP fault, SW Anatolia. Earth and Planetary Science Letters 498: 101-115. https://doi.org/10.1016/j.epsl.2018.06.022

Keller EA (1977). Adjustments of drainage to bedrock in regions of contrasting tectonic framework. Geological Society America Abstract Programs USA 9: 1046.

Keller EA (1986). Investigation of active tectonics: use of surficial earth processes. In: Active tectonics, National Academy Press 8: 136-147.

Keller EA, Pinter N (2002). Active tectonics: earthquakes, uplift, and landscape, second edition. Prentice Hall, New Jersey p. 362.

Kirby E, Whipple KX (2001). Quantifying differential rock-uplift rates via stream profile analysis. Geology 29 (5): 415-418. https://doi.org/10.1130/0091-7613(2001)029<0415:QDRURV>2.0.CO;2.

Kirby E, Whipple KX (2012). Expression of active tectonics in erosional landscapes. Journal of Structural Geology 44: 54-75. https://doi.org/10.1016/j.jsg.2012.07.009

Kirby E, Whipple KX, Tang W, Chen Z (2003). Distribution of active rock uplift along the eastern margin of the Tibetan Plateau: Inferences from bedrock channel longitudinal profiles. Journal of Geophysical Research: Solid Earth 108 (B4): 1-24 https://doi.org/10.1029/2001JB000861

Kreemer C, Blewitt G, Klein EC (2014). A geodetic plate motion and Global Strain Rate Model. Geochemistry, Geophysics, Geosystems 15 (10): 3849-3889. https://doi.org/10.1002/2014GC005407

Lague D, Davy P (2003). Constraints on the long-term colluvial erosion law by analyzing slope-area relationships at various tectonic uplift rates in the Siwaliks Hills (Nepal). Journal of Geophysical Research: Solid Earth 108 (B2). https://doi.org/10.1029/2002JB001893

Le Pichon X, Angelier J (1979). The Hellenic Arc and trench system: a key to the evolution of the eastern Mediterranean area. Tectonophysics 60: 1-42. https://doi.org/10.1016/0040-1951(79)90131-8

Marinoni O (2004). Implementation of the analytical hierarchy process with VBA in ArcGIS. Computers and Geosciences 30 (6): 637-646. http://dx.doi.org/10.1016/j.cageo.2004.03.010

Marinos P, Hoek E (2001). Estimating the geotechnical properties of heterogeneous rock masses such as flysch. Bulletin of Engineering Geology and the Environment 60 (2): 85-92. https://doi.org/10.1007/s100640000090

McKenzie D (1972). Active tectonics of the Mediterranean region. Geophysical Journal International 30 (2): 109-185. https://doi.org/10.1111/j.1365-246X.1972.tb02351.x

McKenzie D (1978). Active tectonics of the Alpine-Himalayan belt: the Aegean Sea and surrounding regions. Geophysical Journal International 55 (1): 217-254. https://doi.org/10.1111/j.1365-246X.1978.tb04759.x

Merritts D, Vincent KR (1989). Geomorphic response of coastal streams to low, intermediate and high rates of uplift, Mendocino triple junction region, northern California. Geological Society of America Bulletin 101: 1373-1388. https://doi.org/10.1130/0016-7606(1989)101<1373:GROCST>2.3.CO;2

Meulenkamp JE, Wortel WJR, Van Wamel WA, Spakman W, Strating EH (1988). On the Hellenic Subduction Zone and the Geodynamic Evolution of Crete in the Late Middle Miocene. Tectonophysics 146: 203-215. https://doi.org/10.1016/0040-1951(88)90091-1

Ocakoğlu N (2012). Investigation of Fethiye-Marmaris Bay (SW Anatolia): seismic and morphologic evidences from the missing link between the Pliny Trench and the Fethiye-Burdur Fault Zone. Geo-Marine Letters 32: 17-28. https://doi.org/10.1007/s00367-011-0234-2

Ouayah M, Namous M, Ourribane M, Elaloui A, Krimissa S et al. (2021). Assessment of relative tectonic activity using morphotectonic analysis in the Central High Atlas, Demnate Region, Morocco. Arabian Journal of Geosciences 14 (9): 813. https://doi.org/10.1007/s12517-021-07126-y

Önalan M (1979). Elmalı-Kaş (Antalya) arasındaki bölgenin jeolojisi. İ.Ü. Fen Fakültesi Monografileri, 29. İstanbul, Ph.D. Thesis, l40 pp (unpublished) (in Turkish).

Över S, Özden S, Yilmaz H, Pınar A, Ünlügenç UC et al. (2013). Plio-Quaternary stress regime in Eşen Çay Basin, SW Turkey. Geological Society, London, Special Publications 372 (1): 547-560. https://doi.org/10.1144/SP372.1

Pérez-Peña JV, Azor A, Azañón JM, Keller EA (2010). Active tectonics in the Sierra Nevada (Betic Cordillera, SE Spain): Insights from geomorphic indexes and drainage pattern analysis. Geomorphology 119 (1-2): 74-87. https://doi.org/10.1016/j.geomorph.2010.02.020

Pike RJ, Wilson SE (1971). Elevation-relief ratio, hypsometric integral, and geomorphic area-altitude analysis. Geological Society of America Bulletin 82 (4): 1079-1084. https://doi.org/10.1130/0016-7606(1971)82[1079:ERHIAG]2.0.CO;2

Ramírez-Herrera MT (1998). Geomorphic assessment of active tectonics in the acambay graben, Mexican volcanic belt. Earth Surface Processes and Landforms: The Journal of the British Geomorphological Group 23 (4): 317-332. https://doi.org/10.1002/(SICI)10969837(199804)

Rockwell TK, Keller EA, Johnson DL (1985). Tectonic geomorphology of alluvial fans and mountain fronts near Ventura, California. In Tectonic Geomorphology. Proceedings of the 15th Annual Geomorphology Symposium. Allen and Unwin Publishers, Boston, MA, pp. 183-207.

Saaty L (1977). A scaling method for priorities in hierarchical structures. Journal of Mathematical Psychology 15: 234–281. https://doi.org/10.1016/0022-2496(77)90033-5

Schwanghart W, Scherler, D (2014). TopoToolbox 2–MATLAB-based software for topographic analysis and modeling in Earth surface sciences. Earth Surface Dynamics 2 (1): 1-7.

Sharma G, Mohanty S (2018). Morphotectonic analysis and GNSS observations for assessment of relative tectonic activity in Alaknanda basin of Garhwal Himalaya, India. Geomorphology 301: 108-120. https://doi.org/10.1016/j.geomorph.2017.11.002

Silva PG, Goy JL, Zazo C, Bardajı T (2003). Fault-generated mountain fronts in southeast Spain: geomorphologic assessment of tectonic and seismic activity. Geomorphology 50 (1-3): 203-225. https://doi.org/10.1016/S0169-555X(02)00215-5

Strahler AN (1952). Hypsometric (area-altitude curve) analysis of erosional topography. Geological Society of America Bulletin 63: 1117-1141. https://doi.org/10.1130/0016-7606(1952)63[1117:HAAOET]2.0.CO;2

Şenel M (1994). Geological Map of Fethiye, M9 quadrangle, in 1:100.000 scale sheet. General Directorate of Mineral Research and Exploration, Ankara, Turkey (in Turkish).

Şenel M (1997). Geological Map of Fethiye, L8 quadrangle, in 1:100.000 scale sheet. General Directorate of Mineral Research and Exploration, Ankara, Turkey (in Turkish).

Şenel M (2002). Geological Map of Turkey, Denizli 1:500.000 scale sheet. General Directorate of Mineral Research and Exploration, Ankara, Turkey (in Turkish).

Şenel M, Selçuk H, Bilgin ZR, Şen MA, Karaman T et al. (1989). Geology of the Region around Çameli (Denizli)-Yeşilova (Burdur)-Elmalı (Antalya). General Directorate of Mineral Research and Exploration. Report No. 9429. Unpublished (in Turkish).

Snyder NP, Whipple KX, Tucker GE, Merritts DJ (2000). Landscape response to tectonic forcing: Digital elevation model analysis of stream profiles in the Mendocino triple junction region, northern California. Geological Society of America Bulletin 112 (8): 1250-1263. https://doi.org/10.1130/0016-7606(2000)112<1250:LRTTFD>2.0.CO;2

Tarboton DG, Bras RL, Rodriguez-Iturbe I (1989). Scaling and elevation in river networks. Water Resources Research 25 (9): 2037-2051. https://doi.org/10.1029/WR025i009p02037

Taesiri V, Pourkermani M, Sorbi A, Almasian M, Arian M (2020). Morphotectonics of Alborz Province (Iran): A case study using GIS method. Geotectonics 54: 691-704.

Taymaz T, Price S (1992). The 1971 May 12 Burdur earthquake sequence, SW Turkey: a synthesis of seismological and geological observations. Geophysical Journal International 108 (2): 589-603. https://doi.org/10.1111/j.1365-246X.1992.tb04638.x

ten Veen JH (2004). Extension of Hellenic forearc shear zones in SW Turkey: the Pliocene-Quaternary deformation of the Esen Cay Basin. Journal Geodynamics 37: 181-204. https://doi.org/10.1016/j.jog.2004.02.001

Tosun L, Avşar U, Avşar Ö, Dondurur D, Kaymakçı N (2021). Active tectonics and kinematics of Fethiye-Göcek Bay, SW Turkey: Insight about the eastern edge of Pliny-Strabo Trenches. Journal of Structural Geology 145: 104287. https://doi.org/10.1016/j.jsg.2021.104287

Troiani F, Della Seta M (2008). The use of the stream length–gradient index in morphotectonic analysis of small catchments: a case study from Central Italy. Geomorphology 102: 159-168. https://doi.org/10.1016/j.geomorph.2007.06.020

Tur H, Yaltırak C, Elitez İ, Sarıkavak KT (2015). Pliocene–Quaternary tectonic evolution of the Gulf of Gökova, southwest Turkey. Tectonophysics 638: 158-176. https://doi.org/10.1016/j.tecto.2014.11.008

Whipple KX (2004). Bedrock rivers and the geomorphology of active orogens. Annual Review of Earth and Planetary Sciences 32: 151-185. https://doi.org/10.1146/annurev.earth.32.101802.120356

Whipple KX, Tucker GE (1999). Dynamics of the stream-power river incision model: Implications for height limits of mountain ranges, landscape response timescales, and research needs. Journal of Geophysical Research: Solid Earth 104 (B8): 17661-17674. https://doi.org/10.1029/1999JB900120

Willgoose G, Hancock G (1998). Revisiting the hypsometric curve as an indicator of form and process in transport-limited catchment. Earth Surf Process Land 23 (7): 611-623. https://doi.org/10.1002/(SICI)1096-9837(199807)23:7<611::AID-ESP872>3.0.CO;2-Y

Wobus C, Whipple KX, Kirby E, Snyder N, Johnson J et al. (2006). Tectonics from topography: procedures, promise, and pitfalls. In: Willett, S., et al., eds., Tectonics, Climate, and Landscape Evolution: Geological Society of America Special Paper 398: 55-74. https://doi.org/10.1130/2006.2398(04)

Woodside J, Mascle J, Huguen C, Volkonskaia A (2000). The Rhodes Basin, a post-Miocene tectonic trough. Marine Geology 165: 1-12. https://doi.org/10.1016/S0025-3227(99)00140-1

Yaltırak C, Elitez İ, Aksu A, Hall J, Çifci G et al.(2010). The relationship and evolution of the Burdur-Fethiye Fault/Shear Zone, the Rhode Basin, Anaximander Seamounts, the Antalya Gulf, and the Isparta Angle since Miocene to Recent in tectonics of the Eastern Mediterranean. In: 63th Geology Congress of Turkey, 5-9 April 2010. Ankara.

Yılmaz Y, Genç SC, Gürer F, Bozcu M, Yılmaz K et al. (2000). When did the western Anatolian grabens begin to develop? In: E. Bozkurt, J.A. Winchester, J.D.A. Piper (Eds.), Geological Society, London, Special Publications 173: 353-384. https://doi.org/10.1144/GSL.SP.2000.173.01.17

Zitter TA, Woodside JM, Mascle J (2003). The Anaximander Mountains: a clue to the tectonics of southwest Anatolia. Geological Journal 38 (3-4): 375-394. https://doi.org/10.1002/gj.961